**Quantification Techniques for Arterial Blood Flow and the Left Atrium**

by

Nikhil Jha

A thesis submitted to the Graduate Faculty of
Auburn University
in partial fulfillment of the
requirements for the Degree of
Master of Science

Auburn, Alabama
August 2, 2014

Keywords: Magnetic Resonance Imaging, Pulse Wave Velocity,
Arterial Blood Flow, Left Atrial Volumetric Analysis.



Approved by

Thomas S. Denney, Jr., Chair, Professor of Electrical and Computer Engineering
Stanley J. Reeves, Professor of Electrical and Computer Engineering
Gopikrishna Deshpande, Assistant Professor of Electrical and Computer Engineering

**Abstract**

Cardiovascular dysfunction is a major cause of morbidity and mortally. As such, the characterization of the heart and surrounding vessels has a high clinical significance. The advent of cardiac magnetic resonance imaging (MRI) has provided an effective and efficient, noninvasive method of looking at the cardiovascular system.

This thesis investigates the application of MRI in the quantification of two particular aspects of the cardiovascular system: arterial blood flow and the left atrium (LA).

The use of pulse wave velocity (PWV) in flow quantification is explored. The majority of prevalent techniques use landmarks in the time-domain to calculate PWV. However, this presents problems with reliability due to the low temporal resolution of MRI flow data. A frequency-domain based approach through the use of the Fourier transform is investigated. This method is shown to be effective in minimizing errors found in the time-domain calculations.

Dual-contour propagation is a post-processing technique used to produce contours. This is done through the propagation of manually drawn end-diastole (ED) and end-systole (ES) contours throughout the cardiac cycle. The method has been previously validated in regards to its applicability for ventricular data. The application of this technique with LA MRI images is considered and shown to be a valid propagation method.

Finally, different approaches to volumetric quantification of the LA are explored. Issues are raised with the accepted serial short-axis and area-length calculation methods and a new virtual short-axis method is proposed. This method seeks to compensate for the inaccurate geometric assumptions made by the area length method whilst avoiding the time intensive use of the short-axis in quantification. This method is shown to be effective and efficient method for volumetric analysis.

**Acknowledgments**

First and foremost, I would like to thank Dr. Thomas S. Denney Jr. From my time as an undergraduate, he has afforded me great opportunities through the Auburn University MRI Research Center. From his instruction on MATLAB to teaching me to use the MRI machines, he has made this work possible. His wisdom and insight have guided me in my work and helped me explore the field of cardiovascular MRI. His enthusiasm for the research has helped cultivate a profound fascination with the subject.

Dr. Nouha Salibi has been both an invaluable resource and a constantly uplifting presence during my time at Auburn. Her comprehensive knowledge of MRI has helped me overcome many roadblocks.

I would also like to thank my advisory committee: Dr. Gopikrishna Desphande and Dr.Stanley J. Reeves for their support in my thesis and my work.

Alongside them, the doctors and researchers at the University of Alabama at Birmingham School of Medicine have helped make this work possible. Their help and guidance, particularly that of Dr. Himanshu Gupta and Dr. Steven S Lloyd, has been vital to my work in cardiovascular research.

My coworkers and labmates: Wei Zha, Chun Schiros, Ming Li, Wayne Duggan, and Xiaoxia Zhang, have been absolutely incredible. Both professionally and personally, they have created an environment in which I have truly loved working. I would especially like to thank Wei for her support and immense involvement when I first joined the research group. Without this help, I would still be trying to figure out coding in MATLAB. I also want to particularly thank Xiaoxia Zhang. Without her sacrificing nights and weekends to spend hours scanning subjects, I would not have been able to obtain data.

I would like to thank Ms. Linda Baressi and the workers at the Broun Hall Machine Shop. Working there has allowed to me to step back and take a breath at times of incredible frustration. Miss Linda is an incredible and constant source of support and inspiration.

My family, my parents and brother, have provided unconditional love and support in all my endeavors. Without their presence in my life and the wonderful upbringing they provided, I would not be who I am and certainly not have been able to get thus far.

Finally, I would like to thank my grandparents, Dr. Ashutosh Mishra and Dr. Shankuntala Mishra. Their presence during my time at Auburn has brought me unspeakable joy. Their immense love, constant support, and unending encouragement have been a driving force in helping me overcome my obstacles. I dedicate this thesis to them.

## Table of Contents

## List of Tables

## List of Figures

## List of Abbreviations

| | |
|---|---|
| 2ch | Two-Chamber |
| 4ch | Four-Chamber |
| AL | Area-Length |
| AV | Atrioventricular |
| cMRI | Cardiac Magnetic Resonance Imaging |
| CT | Computed Tomography |
| ED | End-Diastole |
| ES | End-Systole |
| IRB | Institutional Review Board |
| LV | Left Ventricle |
| LA | Left Atrium |
| MPA | Main Pulmonary Artery |
| MRI | Magnetic Resonance Imaging |
| MV | Mitral Valve |
| NIH | National Institute of Health |
| NMR | Nuclear Magnetic Resonance |
| NRR | Non-Rigid Registration |
| PC | Phase Contrast |
| PET | Positron Emission Tomography |

| | |
|---|---|
| PWV | Pulse Wave Velocity |
| RA | Right Atrium |
| RF | Radio Frequency |
| ROI | Region of Interest |
| RPA | Right Pulmonary Artery |
| RV | Right Ventricle |
| SA | Short-Axis |
| SSA | Serial Short-Axis |
| SPAMM | Spatial Modulation of Magnetization |
| VSA | Virtual Short-Axis |
| VTC | Volume-Time Curve |

# Chapter 1

## Introduction

The term cardiology often invokes the image of the human heart and its four chambers. The surrounding vessels, however, play an integral role and, together with the heart, form the cardiovascular system. In a system, the characteristics of a specific component impact the other components. This is no different for the cardiovascular system. The characteristics and dysfunctions of individual anatomies have a cascading affect and cause changes in the rest of the cardiovascular system. It is important to recognize that the characteristics of the individual anatomical components are not static. As they are composed of, among other things, various muscle and elastic tissues, their attributes change in response to variations in pressure, encompassed blood volume, etc. The heart remodels with age and disease, the chambers changing in size and shape; the arteries can lose elasticity and harden; there are changes in blood flow around the body. As such, it is important to quantify the relationships between the various anatomies of this system and how their overall characteristics change with the onset of physiological dysfunction concentrated on one or more of the components. This is further compelling due to the crucial role that the cardiovascular system plays in overall health.

However, before being able to characterize the overall cardiovascular system, it is necessary to quantify the individual components. With the advent of noninvasive imaging technology, it has become possible to observe, quantify, and characterize the behavior of the various chambers and vessels in vivo. Magnetic resonance imaging (MRI) has been shown to be one of the most effective tools in achieving this. It has, in fact, been used extensively in both research and clinical settings.

There has been extensive work to quantify some targeted anatomies such as the left ventricle (LV). Less work has been done to effectively measure some of the other components of the cardiovascular system. As more knowledge arises about them, the quantification of these components has become significant. In this thesis, the focus is on the methods for processing and quantification for two specific anatomical structures: the arterial system and the left atrium (LA).

In regards to the arterial system, the prevalent methods for blood flow quantification are discussed and an alternative method is presented. These methods are then compared for their accuracy, efficiency and reliability.

For the LA, the applicability of post-processing techniques previously used in the ventricles is explored. The various methods for the LA volume quantification are then described and a novel method is proposed. The validity and performance of this new method will be analyzed.

Finally, the work will be summarized and future work regarding the application of these individual anatomical characterizations to quantification of the more comprehensive cardiovascular system.

# Chapter 2

## Overview of the Cardiovascular System

The cardiovascular system is one of the major systems of the human body. It is responsible for the transport of oxygen and various nutrients throughout the body via the pumping of blood. This system consists of the heart and blood vessels.

### 2.1 The Heart

#### 2.1.1 Cardiac Anatomy

The heart is a hollow, conical, muscular organ approximately the size of a human fist. Weighing between 250 and 350 grams, it is located in the medial cavity of the thorax between the lungs [1]. It rests within the pericardium, which is a double walled sac.

The heart itself consists of four chambers: two atria, which receive blood into the heart, and two ventricles, which discharge the blood as shown in Figure 2.1. It is also separated into two sides, the left and the right, separated by the septum. Each side consists of a superior atrium and inferior ventricle separated by a valve. The right side deals with deoxygenated blood; the right atrium (RA) receiving it from the body and then the right ventricle (RV) pushing it towards the lungs for oxygenation via the pulmonary valve. The left side deals with oxygenated blood; the left atrium (LA) receives the blood from the lungs and the left ventricle (LV) expelling it to the rest of the body through the aortic valve. Between the atria and ventricles lie the atrioventricular (AV) valves. The semilunar valves exist between the ventricles and the adjacent arteries. The two semilunar valves are the pulmonary valve, between the RV and pulmonary artery, and the aortic valve, between the LV and aorta.

The cardiac wall itself consists of three layers. The innermost layer, the endocardium, is a thin membranous lining of the chambers as well as a covering for the fibrous valve skeletons. The myocardium, the middle layer, is composed of cardiac muscle and is responsible for the contractile

motion of the heart. Lastly, the superficial epicardium consists mainly of connective tissue and serves to protect the underlying cardiac muscle.

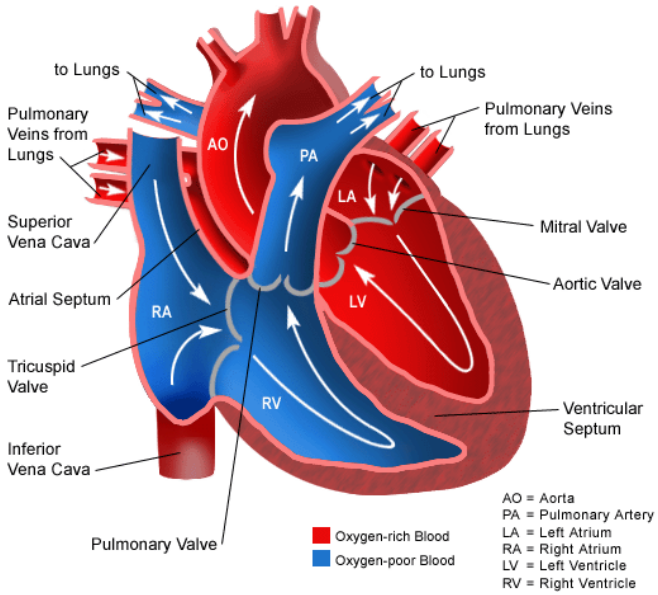


Figure 2.1: Anatomy of a Normal Heart [2].

### 2.1.2 Cardiac Physiology

The heart contracts rhythmically with the resulting impetus pushing blood throughout the cardiovascular system. A complete contraction and relaxation of the heart is considered one cardiac cycle and takes approximately 800ms. A heartbeat corresponds to a single cardiac cycle with the average human adult completing approximately 70 beats per minute [1].

The complete cardiac cycle consists of three phases dictated by the contraction (systole) and relaxation (diastole) of various anatomies. The first phase, atrial systole, consists of contraction of the atria. As the AV valves are open and the semilunar valves are closed, this results in blood flowing from the atria into the ventricles. After this phase, ventricular systole occurs. In this phase the ventricles contract while the atria relax, resulting in closure of the AV valves whiles the pulmonary and aortic valves open. This results in blood being expelled from the ventricles into the pulmonary arteries and the

aorta. The last phase, isovolumetric relaxation, occurs when there is an overall relaxation of the heart. The result of this is the closure of the semilunar valves and the filling of the atria with blood from the vena cava and pulmonary veins [3]. This process is illustrated in Figure 2.2.

This activity is incited by electrical impulses originating in the sinoatrial and AV nodes. Cardiac muscle has an intrinsic ability to depolarize and contract on its own but the heart is also connected to the autonomic nervous system which can alter cardiac rhythm.

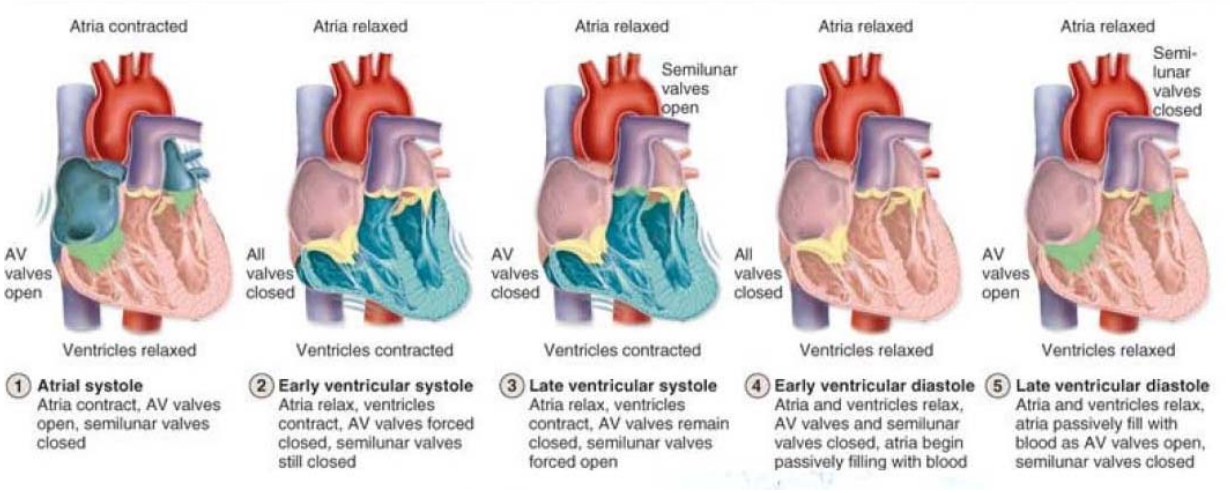


Figure 2.2: The Cardiac Cycle [4].

## 2.2 Blood Vessels

### 2.2.1 Vascular Anatomy

There are three major types of blood vessels in the body. These are arteries, veins, and capillaries. Arteries carry blood away from the heart while veins carry blood towards the heart. Capillaries are sites for direct cellular exchange between the blood and the tissues surrounding the capillaries. Almost all of the arteries carry oxygenated blood and almost all the veins carry deoxygenated blood. The only exceptions are those of the pulmonary circuit, where the pulmonary artery carries deoxygenated blood while the pulmonary vein carries oxygenated blood.

The major blood vessels have similar wall composition surrounding the blood-filled lumen. Vessel walls have three distinct layers. The innermost layer, the tunica intima, contains the endothelium which lines the lumen. The middle layer, the tunica media, is composed of smooth muscle cells and elastin. This layer is responsible for vasoconstriction, vasodilation, and provides the elasticity characteristic of the major blood vessels. Finally the tunica externa is the outermost layer and composed almost entirely of fibrous collagen. It serves to protect, reinforce, and anchor the blood vessels. This anatomy is shown in Figure 2.3.

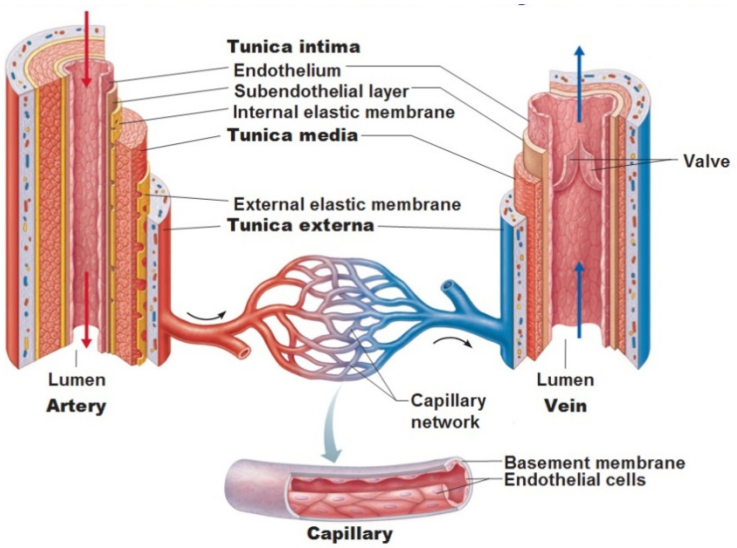


Figure 2.3: Blood Vessel Structure [5].

### 2.2.2 Vascular Physiology

Blood vessels form a closed loop circuit in order to circulate blood throughout the body. These loops can be considered to begin and end at the heart. The order of blood vessels is always consistent. Circulation begins from the arteries, which branch into subsequently smaller arterioles, flows through the capillary beds, and then to small venules which conglomerate into the major veins, thus returning the blood to the heart.

There are two main circulations when it comes to the circulatory system. These are the systemic circulation and the pulmonary circulation. The general circulation begins at the LV, which expels

oxygenated blood into the aorta. This blood is then carried through the core of the body and extremities, where it is subsequently deoxygenated and returned to the right atrium via the veins. The pulmonary circulation begins at the RV. The RV discharges deoxygenated blood into the pulmonary arteries, which lead to the pulmonary capillaries. The blood is then oxygenated due to action from the lungs, and then travels through the pulmonary veins into the LA. These circulations can be seen in Figure 2.4.

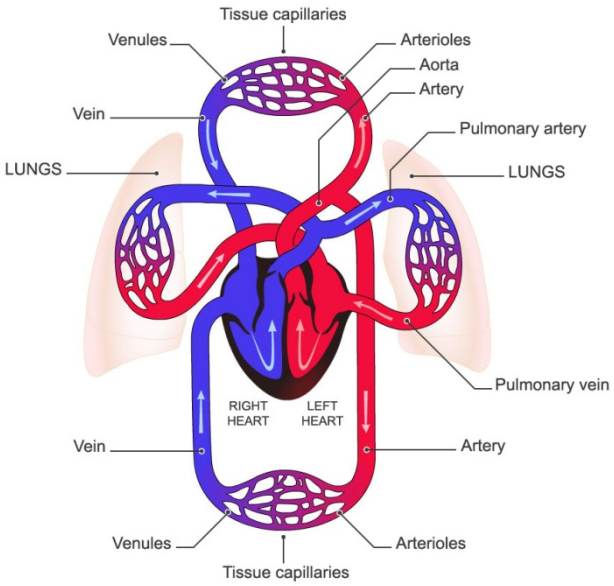


Figure 2.4: Circulatory System [6].

### 2.3 Cardiovascular Dysfunction

According to the National Institute of Health (NIH), cardiovascular disease causes approximately 17.5 million deaths each year. This makes it the leading cause of deaths, accounting for over 30% of deaths worldwide [7]. The term applies to a host of diseases and dysfunctions that involve the heart and surrounding vasculature. The causes of these may be genetic, environmental, a result of personal habits, among others.

One of the more common cardiovascular issues is heart failure. This is defined by the inability of the heart to circulate blood effectively. This may be caused by a variety of dysfunctions such as heart attacks, valve diseases, or hypertension, among others [8].

A common source of cardiovascular dysfunction is arteriosclerosis. This is where the walls of the arteries become thicker and stiffened, resulting in hypertension. This dysfunction can affect the flow of blood and thus have a negative impact on the cardiovascular system as a whole [1].

# Chapter 3

## Overview of Cardiovascular Magnetic Resonance Imaging

There are many imaging modalities used to asses cardiac function. These include x-ray, computed tomography (CT), and positron emission tomography (PET), all of which require ionized electromagnetic radiation. Modalities that do not require ionized electromagnetic radiation include ultrasound and MRI. The use of MRI to assess cardiac parameters has become increasingly standard both in research and clinically. This is because, along with being non-ionizing and non-invasive, it is a very versatile tool that allows for a much clearer picture of the cardiovascular system. Using the different techniques of cMRI, we can look at anatomy, measure blood flow, and evaluate tissue motion.

### 3.1 Fundamentals of Magnetic Resonance Imaging

Magnetic resonance imaging uses the phenomenon of nuclear magnetic resonance (NMR) to excite protons in hydrogen atoms. Hydrogen is used as is one of the most abundant elements in the human body, found in both water and fat, and is exceptionally sensitive to magnetic resonance.

When a large, external, uniform magnetic field $B_0$ is applied, the proton spins align along the axis of the field identified as the $z$ direction. In this case the system is in a state of equilibrium, in which the net magnetization $M_0$ is aligned with $B_0$ in the $z$ direction. These proton spins precess at a Larmor frequency $\omega = \gamma B_0$, where $\gamma$ is the gyromagnetic ratio. This ratio has a constant value of 42.58 MHz/Tesla for protons.

A radio frequency (RF) pulse is applied to create a second magnetic field $B_1$, perpendicular to $B_0$, and shift the system into an excited state. This adds a transverse element to the net magnetization which can now be resolved into two components: $M_z$, the longitudinal component along the original axis, and $M_{xy}$, the transverse component. The properties of the RF pulse determine the amount of magnetization and the flip angle α. After the pulse is applied, the protons enter the relaxation stage, whereupon they return to

the state of equilibrium. As a proton precesses around $B_0$, the rotation of the transverse signal produces a measurable current in a proximal RF coil. This process is illustrated in Figure 3.1.

There are two types of relaxation: spin-spin relaxation, which corresponds to the decay of $M_{xy}$, and spin-lattice relaxation, which corresponds to the recovery of $M_z$. Their respective time constants are $T_1$ and $T_2$. Different tissues have different time constants, thus allowing for a source of contrast in MR images.

A particular slice selection is imaged through use of the basic principles NMR. A gradient field is applied in the *z* direction so that only a particular slice will be exposed to the resonant frequency and will experience excitation. Spatial localization is done through two mechanisms: phase encoding and frequency encoding. Phase encoding occurs when a gradient magnetic field is applied to the *y* direction. This causes a dephasing of the voxels in the *y* direction. Meanwhile all the voxels along a particular row in the *x* direction will retain the same relative phase. Frequency encoding is applied afterwards where a gradient is applied along the *x* direction, also known as the readout direction. This causes the precession frequencies to vary along the readout direction.

This data obtained after these sequences are interpreted as scans of Fourier space. Using an inverse Fourier transform, a 2D image can be reconstructed.

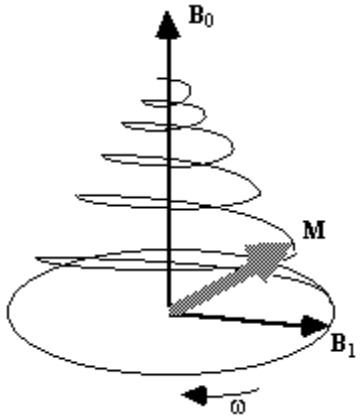


Figure 3.1: Precession of a proton back to equilibrium position after application of $B_1$ [9].

### 3.2 Cardiac Magnetic Resonance Imaging

Cardiac MRI (cMRI) is achieved using a specialized cardiac coil in conjunction with the larger MRI machine. This coil, akin to a chest pad, is placed around the thoracic cavity and allows for more focused imagining of the heart and surrounding vessels. Cardiac imaging can difficult due to the constant motion of the heart. As images are captured over one or more cardiac cycles, artifacts are introduced as a result of both tissue and blood movement. In order to minimize movement, patients are commonly asked to hold their breath for up to 20 seconds after exhaling completely in order avoid respiratory artifacts and to keep the heart in a consistent location for imaging.

Using cMRI, we can obtain a large variety of data that pertains to both the structure and function of the cardiovascular system. The particular data acquired varies depending on the imaging protocol used during the MRI. The three most commonly used protocols are cine, tagged, and phase contrast (PC) MRI.

#### 3.2.1 Cine Cardiac MRI

The most used protocol for cardiac imaging is cine cMRI. This protocol uses the basic techniques of MRI explained above in order to obtain images of the heart. The majority of the images fall along two major axes. These are the long axis, which extends lengthwise from the apex to the base of the heart, and the short axis (SA), which is perpendicular to the long-axis and roughly perpendicular to the valve plane. Cardiac MRI allows for great versatility in imaging, allowing an operator to obtain a variety of view of the heart, both along the major axes and in oblique planes. The most common studies involve a series of SA image slices along the length of the heart as well as two-chamber (2ch) and four-chamber (4ch) views obtained through radial slicing along the long axis. Figure 3.2 below illustrates this process.

Cine cMRI has many advantages as it allows the imaging of a slice throughout the entire cardiac cycle. This allows a qualitative view of the heart in order to observe any dysfunction. Post-processing of the images also allow quantitative data to be obtained. As dimensions for the image are known through scanner properties, values such as wall thickness and encompassed blood volume can be obtained over the

entire cardiac cycle for each image. This data can be compiled and used to provide a quantitative perspective of cardiac function.

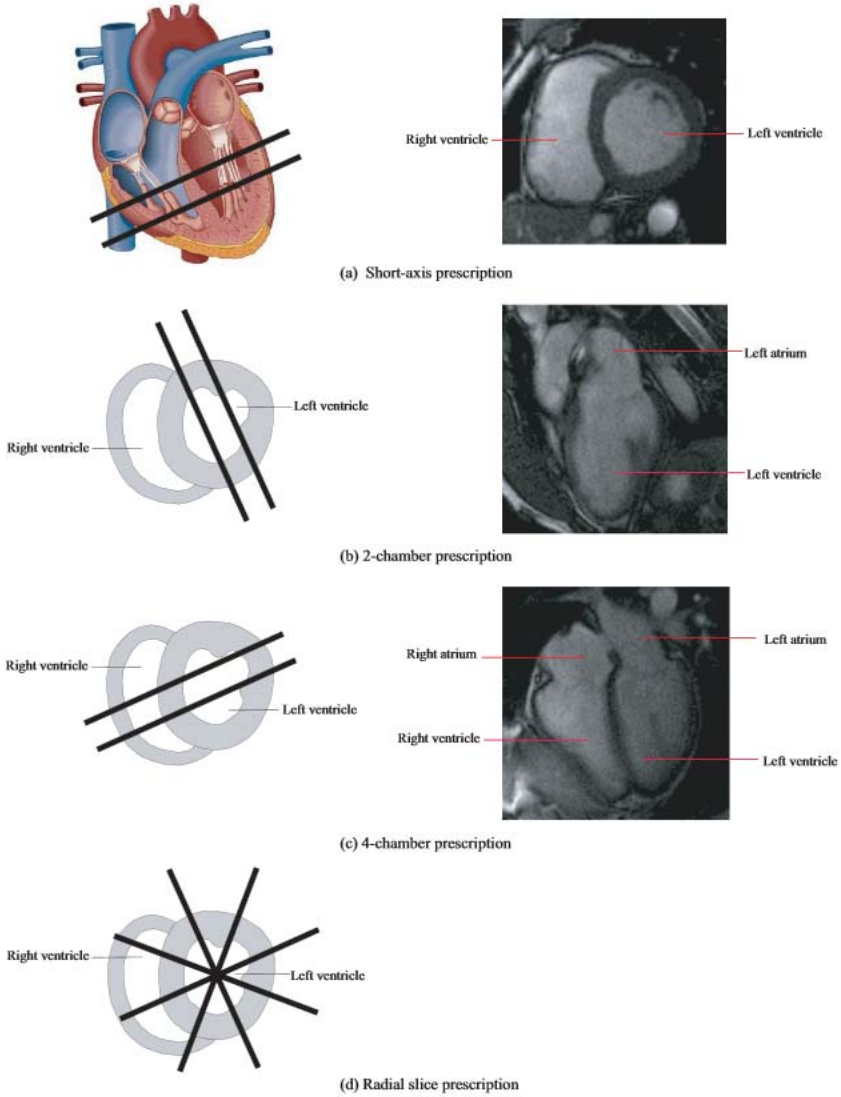


Figure 3.2: Slice prescriptions for cMRI. The images on the left show the prescribed slices represented by the bold lines. The corresponding cMRI images are displayed on the right [10].

### 3.2.2 Tagged Cardiac MRI

Tagged cMRI is a protocol used almost exclusively by the research community due to its post-process heavy nature [11]. While there is lower tissue contrast, tagged cMRI allows for accurate observation of tissue motion.

In tagged cMRI, gridlines are imposed on the underlying myocardial tissue, as shown by Figure 3.3. This is done using a technique known as spatial modulation of magnetization (SPAMM). In this technique, RF pre-pulses are used to cause saturation in the tissue. These patterns of saturation are oriented perpendicular to the image plane. As the cardiac wall deforms as a result of contractile motion, the tags can be seen to deform correspondingly. Due to $T_1$ relaxation, the tag lines fade over the course of the cardiac cycle. As a result, the tags become harder to distinguish in the latter parts of diastole.

Processing of tagged imaging can allow motion to be tracked throughout the cardiac cycle. This allows for derivation of quantitative parameters that relate to the functional nature of the myocardial tissue such as shear, torsion, and rotation.

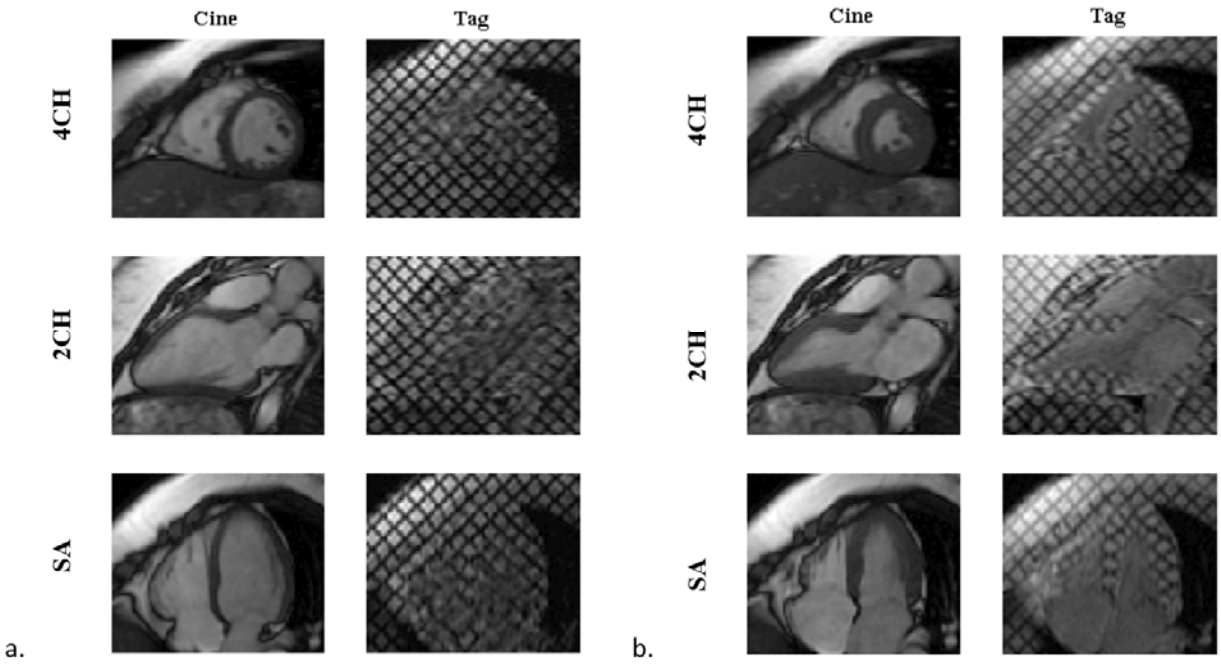


Figure 3.3: Cine and corresponding tagged MR images at ED (a) and ES (b) [12].

### 3.2.3 Phase Contrast Cardiac MRI

PC cMRI differs from both cine and tagged cMRI in that it looks at the flow profile of blood in the cardiovascular system as opposed to solely the structure of the anatomy.

Phase images are obtained using the process of velocity encoding [11]. A flow encoding gradient is used in order to create images that are essentially velocity maps. Protons moving at a constant velocity will undergo a phase shift proportional to the velocity when they are exposed to the gradient. The images are black and white with flow in a particular direction shown in white and the reverse flow shown in black. Stationary tissue is seen as being grey. The intensity of the color corresponds to the velocity and the MRI operator can set a maximum intensity at a particular velocity. Sequences can be made to measure in-plane or through-plane motion. The images obtained can be seen in Figure 3.4.

Obtaining a velocity profile for the cardiovascular system allows data to be gathered regarding flow parameters such as speed and volume. These can be used to further extrapolate more parameters and used in conjunction with other cMRI protocols to obtain data regarding to overall cardiovascular function.

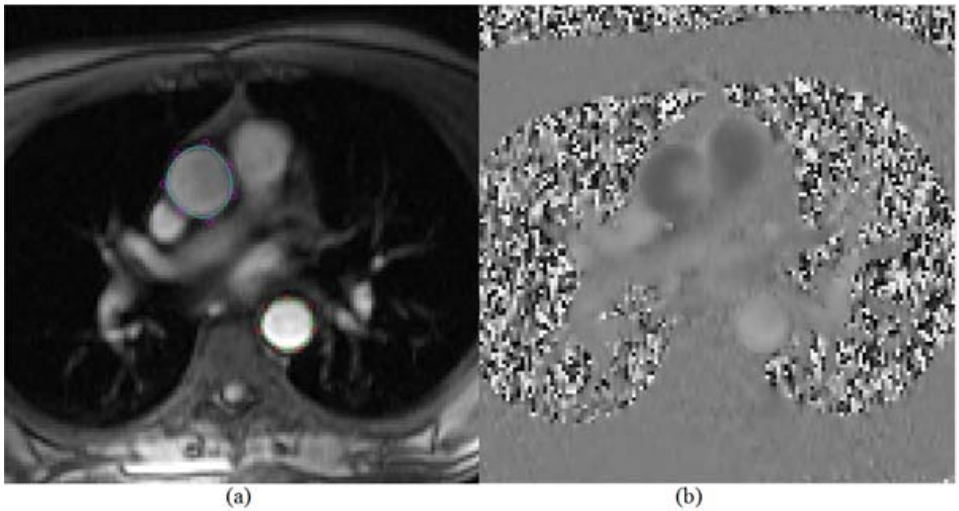


Figure 3.4: Output of PC MRI of transected aorta. Magnitude (a) and corresponding phase (b) images.

# Chapter 4

## Pulse Wave Velocity and the Quantification of Arterial Flow

Blood flow in the arteries is greatly impacted by various cardiovascular events and dysfunction. As such it is important to find an effective and reliable method to quantify blood flow and calculate any changes that occur. The majority of analysis techniques use the time domain to calculate the transit time of blood flow. In this section, a frequency domain approach to this analysis is considered and evaluated. The work in this chapter has been accepted as an abstract in the 20th annual meeting for the International Society of Magnetic Resonance in Medicine [13].

### 4.1 Arterial Flow and Pulse Wave Velocity

#### 4.1.1 Overview of Arterial Flow

Arteries are not just passive conduits through which blood flows. Instead, they constitute a system that regulates pressure, flow, and cardiovascular function. This regulation occurs as a result of arterial capacitance and resistance, which are derived from the structure and quantity of elastin, collagen, and smooth muscle [14]. For an overview of arterial anatomy, refer to Section 2.2.1.

Large arteries such as the aorta can store approximately 50% of the stroke volume during systolic contraction [15]. During diastole, the recoil as a result of elasticity helps drives a continuous blood flow during the diastolic portions of the cardiac cycle. Transmission line models have been proposed, using the electrical transmission line as an analogue to arterial flow [16]. This model is illustrated in Figure 4.1.

The elastic characteristic of an artery is affected by its inherent stiffness. This stiffness impairs the ability for an artery to expand and contract and thus impairs the conversion of pulsatile motion into continuous blood flow. This stiffness is quantified using a measure called pulse wave velocity through a process discussed further in this chapter.

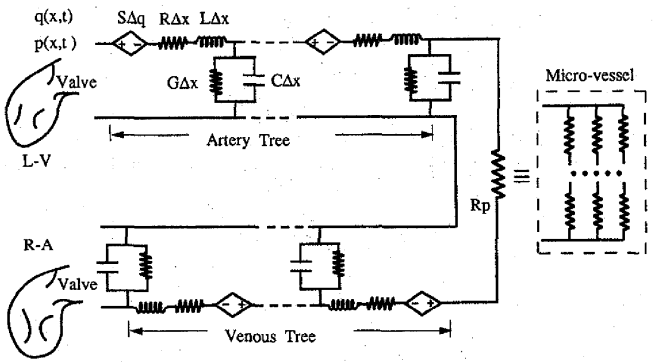


Figure 4.1: Transmission line model for systemic circulation. *R* is resistance, *C* is capacitance, *L* is inductance, and *G* is the leakage (conductance) [16].

### 4.1.2 Significance of Pulse Wave Velocity

Pulse wave velocity is a measure of arterial stiffness. It is related to the incremental elastic modulus, $E_{inc}$, via the Mons-Korteweg equation stated as

$$PWV = \sqrt{\frac{E_{inc} \cdot h}{2r\rho}} \quad (4.1)$$

where $h$ is the vessel wall thickness, $r$ is the vessel radius, and $\rho$ is blood density which has the value 1060 kg/m$^3$ [14]. Using this equation, Bramwell and Hill were able to derive a model relating PWV with distensibility through

$$PWV = \frac{1}{\sqrt{\rho \cdot Distensibility}} \quad (4.2)$$

with the assumption that the vessel is compliant and contains incompressible nonviscous liquid [17]. The calculated distensibility can be further used to find strain using

$$Distensibility = \frac{Strain}{\Delta P} = \frac{\Delta A}{A_{min} \cdot \Delta P} \quad (4.3)$$

where $\Delta P$ is central pulse pressure, $A$ is area of vessel, and $\Delta A = (A_{max} - A_{min})/A_{min}$ [18].

Stiffness is when the distensibility of the arteries decreases thus affecting blood flow. This results in an increase of pressure due to the decreased capacitive effect of the arteries with diminished elasticity. Subsequently, there is an increase in left ventricular properties such as load and mass [19]. There is also

an increase in pressure wave reflection resulting in an increase in systolic pressure, further increasing ventricular load. These changes in the cardiovascular system lead to various dysfunctions.

The increase of stiffness in large arteries can be correlated to a variety of cardiovascular dysfunction and mortality. This is especially true in cases of pre-existing conditions. In diabetic patients, there is a direct correlation between arterial stiffness and cardiovascular mortality [20]. Hypertensive patients have also been found to have an increased PWV that could be directly associated with higher cardiovascular risk [21]. This was corroborated by a large study of hypertensive subjects (n = 1980), which showed an association between arterial stiffness and both cardiovascular and general mortality [22]. Studies of renal disease in patients have also shown that cardiovascular events and mortality correlated with a marked increase in arterial stiffness measured using PWV [23].

The significance of PWV as a measure extends further from sufferers of disease into the general population. A large study (n=2835) showed that in seemingly healthy individuals, stiffness in the arteries is a predictor of cardiovascular dysfunctions such as coronary heart disease [24]. Arterial stiffness as measured by PWV is a risk factor of various cardiovascular issues such as atherosclerosis [25], coronary heart disease [26], hypertension [27], and stroke [28]. In the geriatric population, arterial stiffness was shown to be an indicator or cardiovascular and general mortality [29].

Such findings have highlighted the importance of pulse wave velocity in both clinical and research settings. The information obtained through PWV can be used to evaluate the cardiovascular health of patients as well seeing the affects that various dysfunctions have on the arteries. This is further evidenced by the use of PWV in the guidelines for hypertension treatment by the European Society of Hypertension [30].

### 4.1.3 Calculation of Pulse Wave Velocity

Pulse wave velocity must be calculated and is not obtained from a direct body measurement. It is, in fact, done in two stages: the acquisition stage where the waveform data is collected, and the evaluation stage where the PWV is calculated.

The acquisition of pulse wave data must be done at two points in order evaluate the movement of the wave. This can be done in a variety of ways. The most reliable method is that of cardiac catheterization. This is the most effective method because it provides the most accurate waveform data with high temporal resolution. However, due to its invasive nature, it is not an ideal method to obtain the pulse waveform. Therefore noninvasive methods have been sought in order to obtain the velocity profile. Of these techniques, cMRI is the most effective as it provides a highly resolved image with relatively little noise. The images are obtained using the PC MRI procedure outlined in Section 3.2.3.

The calculation of PWV is no different from any other velocity calculation and is done through the simple formula

$$PWV = \frac{\Delta d}{\Delta t} \quad (4.4)$$

where $\Delta d$ is the distance between the two measurement points and $\Delta t$, known as the transit time, is the time required for the pulse wave to travel. Finding the distance is relatively facile and while specifics depend on the method used to acquire the data, it is essentially just a calculation of distance between the physical data acquisition points. This process involves contouring images using post-processing software and will be further explained in Section 4.2. It is the calculation of transit time that becomes difficult. There are various methods to calculate transit time for cMRI. The majority of these require finding the corresponding points in the two measured waveforms. The time difference between the two points is then used to find the transit time. These methods will be further discussed in Section 4.3. A frequency-based approach to calculate transit time will also be introduced in Section 4.4. The efficacy of these approaches will be further explored throughout this chapter.

### 4.2 Contouring Cardiac Flow Images and Distance Calculation

The post-processing of the images is done through both commercially available software CAAS MR Flow (Pie Medical Imaging, Maastricht, The Netherlands) and custom designed in-house software. However, before data can be obtained, certain regions of interest (ROI) must first be defined. This is because the actual vessels are only a portion of the actual image. Therefore, in order for accurate quantification to occur, the bounds of what the post-processing software will consider relevant have to be set. For blood vessels this is done by the user identifying the vessel in question and edge detection algorithms in the CAAS software defining its inner walls. There is some room for error and as such, the user must manually check that the contours correctly define the vessel. The process is simplified by the fact that, barring a small change in area due to distension, the blood vessels remain a relatively constant circular shape throughout the cardiac cycle. This is all done on the magnitude image, as it provides a clearer picture of the anatomy, and is then transferred to the corresponding phase images. This allows the software to determine flow velocities from the phase images only within the defined area. This process is shown below in Figure 4.2.

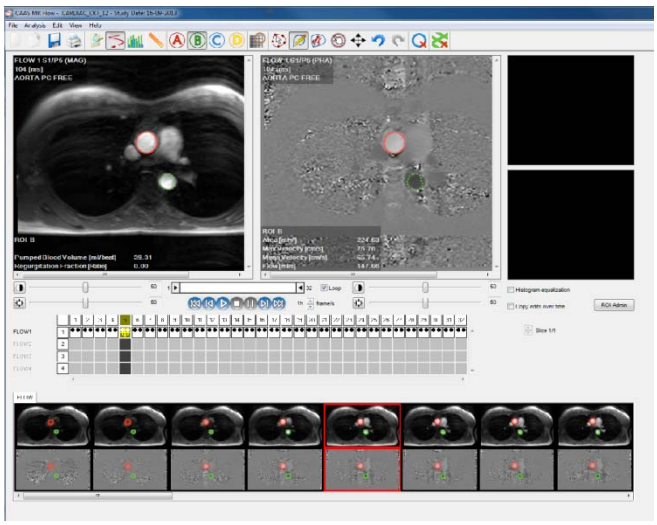

Figure 4.2: Image of contouring the ascending (red) and descending (green) aorta using CAAS MR Flow. The contours are copied to the phase image. In this case the automatic contour for the descending aorta would have to be corrected manually.

In order to find the distance needed in the PWV calculation (Equation 4.4), the images must be further contoured. This is done by using the reference image. This is the image that was used during the MRI scan in order to select the particular slices for the PC MRI. A user can see the slice projections on the reference image, and use that to draw a contour between two of the relevant projections. The software uses this contour to calculate the distance between the points where blood flow was measure. This is illustrated in Figure 4.3.

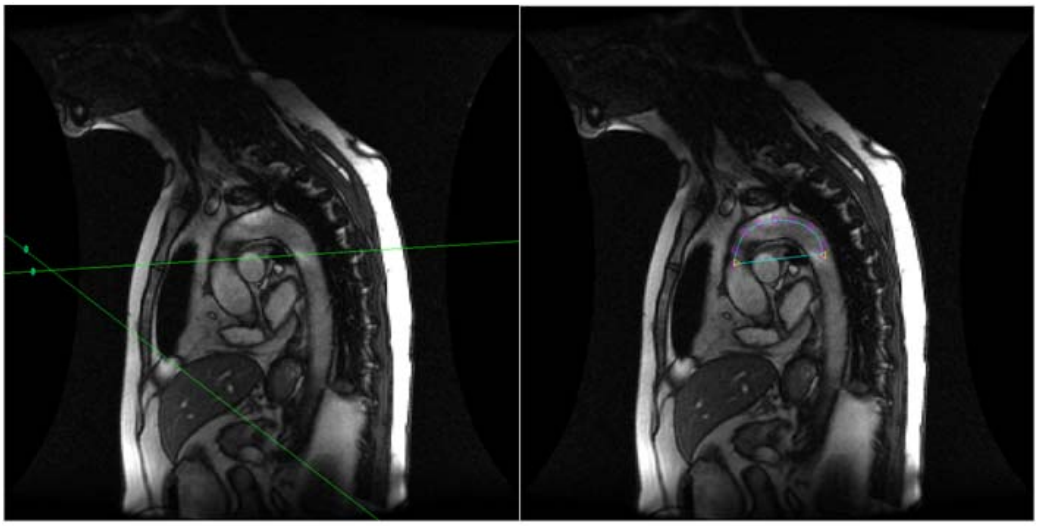


Figure 4.3: Reference image showing slice projections (a) and subsequent contour (b) used to find distance between ascending and descending aorta flow points. Note the contour is drawn to run along the midline of the vessel.

### 4.3 Common Methods for Transit Time Determination

There are a few commonly applied methods to calculate the transit time for PWV. These methods consist almost exclusively of comparing corresponding landmarks at the two flow measurement points in the time domain.

Although the magnitude of the waveform changes as blood flows through the systemic circuit, there is a characteristic shape which allows for determination of distinct landmarks. This waveform change occurs in both normal and dysfunctional cardiovascular systems. The waveform changes can occur due to geometry, such as the curve of the aortic arch which results in impedance changes and

reflected waves, and changes in pressure and flow due to shunting of blood through the branches such as with the carotid and subclavian arteries. It is important to note that this may also introduce noise which can cause difficulties in analysis.

The methods for flow analysis using these landmarks can be seen used for papers in various cardiovascular publications. The majority of these are techniques used originally with ultrasound and catheterization data, which have been subsequently adopted for cMRI use. These include peak analysis, interpolated curves, and onset time analysis.

### 4.3.1 Peak Analysis Using a Quadratic Fit

In quadratic peak analysis, transit time determination is done by comparing the maximums of both measured flows. However, due to the resolution, data may not include the absolute maximum of the flow. Therefore a quadratic is fit to the maximal area and the absolute maximum is determined by that quadratic. By fitting a quadratic to this part of the waveform, the point where flow is at a maximum can be interpolated and its corresponding time can be found. When this is done to both the waveforms, the difference in the two time points can be used to calculate transit time.

This analysis technique was applied using both three points and five points in order to fit a quadratic to the maximal area. This is showing in Figure 4.4. This served as a cursory qualitative check on the applicability of the quadratic function to interpolate the point of maximum flow. While not ideal, the resolution of the data should mean that the shape of the quadratic should not undergo any drastic changes when taking into account five points versus three. Therefore there should not be a drastic change between the transit times calculated by the two methods. If there is a large change in a significant number of studies, it will indicate that a quadratic fit may not accurately represent the shape of the maximal areas in the flow data.

The specific methodology for quadratic fitting is fairly simple. First, the maximal point of the waveform is found. Due to the resolution of PC MRI, this may not represent the true maximum but it will be the closest point to it. Then points from either side of this point are used to create the quadratic. For a

three point quadratic fit, one point on either side is sampled. For a five point fit, two points on either side are used. Using analysis software a quadratic function is realized using these points. Due to the nature of flow waveforms, the quadratic will always be negative, characterized by a downward concavity. Therefore the maximal point will always be the vertex of the function, which in turn provides the relevant time point. This process is repeated for the second waveform. From there, the transit time can be easily calculated as the difference between the two maximal times. This can be applied to Equation 4.4 to find the PWV.

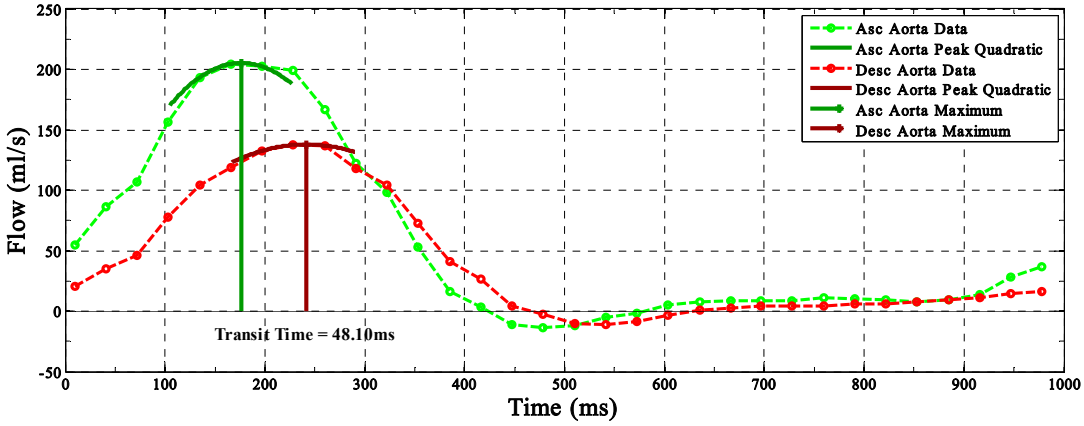


(a)

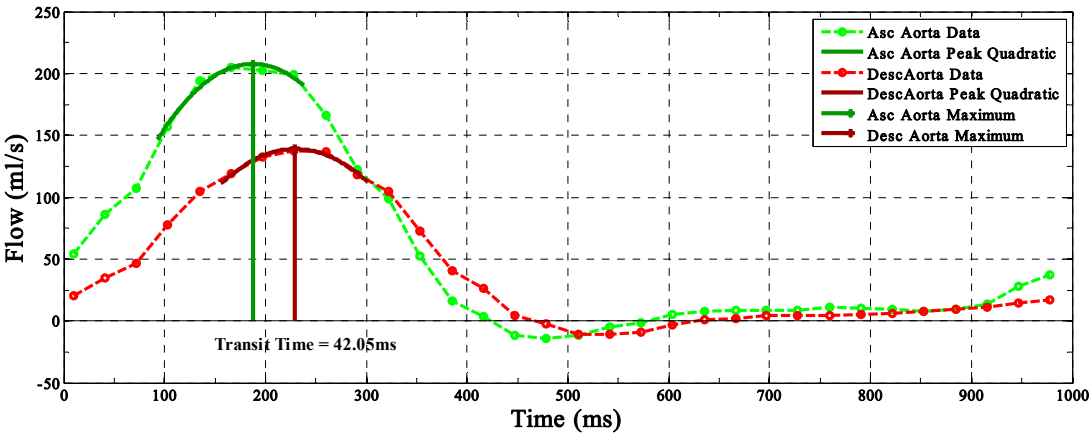


(b)

Figure 4.4: Peak analysis using three-point (a) and five-point (b) quadratic fits

### 4.3.2 Cubic Spline Interpolation of PC MRI Waveforms

Another method to aid in transit time determination is to interpolate more points from the PC MRI data obtained. This allows for more data points to be used as landmarks for comparison between the two waveforms. However, interpolating the data using polynomial parametric curves does not provide data in regards to the behavior of blood in the arteries. This is because data points that are further away still have a large impact on the interpolated curve. Therefore Bezier cubic splines are used to interpolate the data instead, as seen in Figure 4.5 below.

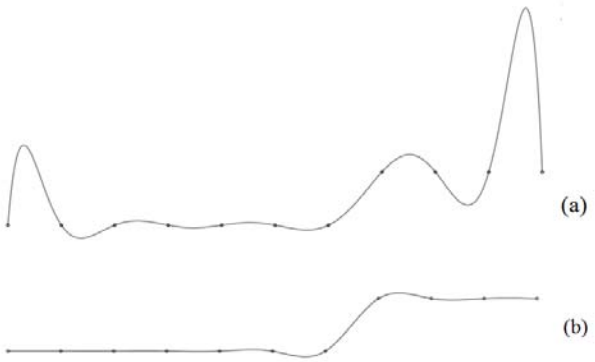


Figure 4.5: Polynomial (a) and spline (b) interpolation of an identical data set [31]. Note the spline interpolation seems more true to the original data points.

In fact, cubic spline interpolation is one of the more common methods to achieve an increase in data points. In this method, cubic polynomial curves are constructed between every two data points in the original set. These curves are combined to create a piecewise function with a continuous second derivative. This allows for minimization of undue influence from distant points and thus creates a fit that is more true to the original data. Most analysis software and coding platforms already contain functions that can interpolate the data. The output of this interpolation is displayed in Figure 4.6. From this point, various landmarks can be selected and compared such as methods similar to the peak analysis in Section 4.3.1 or the commonly used onset time analysis discussed in Section 4.3.2.

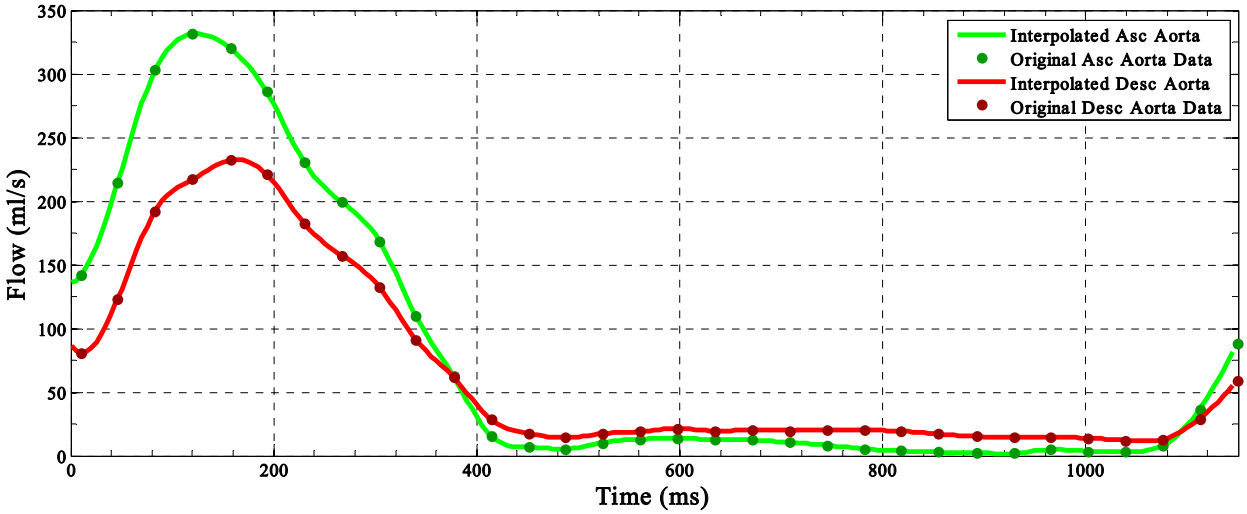

Figure 4.6: Spline interpolation of PC MRI data from ascending and descending aorta.

### 4.3.3 Onset Time Analysis

Transit time determination can also be done through onset time analysis. For onset time analysis, the landmark for comparison is set as a point at which the vascular flow reaches a certain percentage of the maximum flow at each of the measurement points. The difference between the times at which this point is reached on the respective curves is found as the transit time. Methods using values between and including 10 - 20% of the maximum flow can be found in various literature. The reasoning behind this method is that is minimizes the discrepancy caused by using a single peak point. However, this method requires some form of interpolation in order to provide points that will be close to the target value. Spline interpolation is commonly used for this. This method is demonstrated on Figure 4.7 below.

Occasionally there may be issues regarding the offset of the flow curves as data points may actually have a negative value. This is because, during the actual scan itself, flow values can be offset either positively or negatively based on backflow in the artery at time of measurement. Phase errors during PC MRI can also offset the flow, requiring correction. These errors can arise from setting an encoding velocity, during the scan, that is lower than the peak velocity which results in aliasing, or velocity wraparound. Deviation of the image plane due to motion, inadequate spatial resolution, and field

inhomogeneity can also distort flow data [32]. The majority of analysis software allows for correction of this offset by the identification of systole and the shifting of all points based on these points.

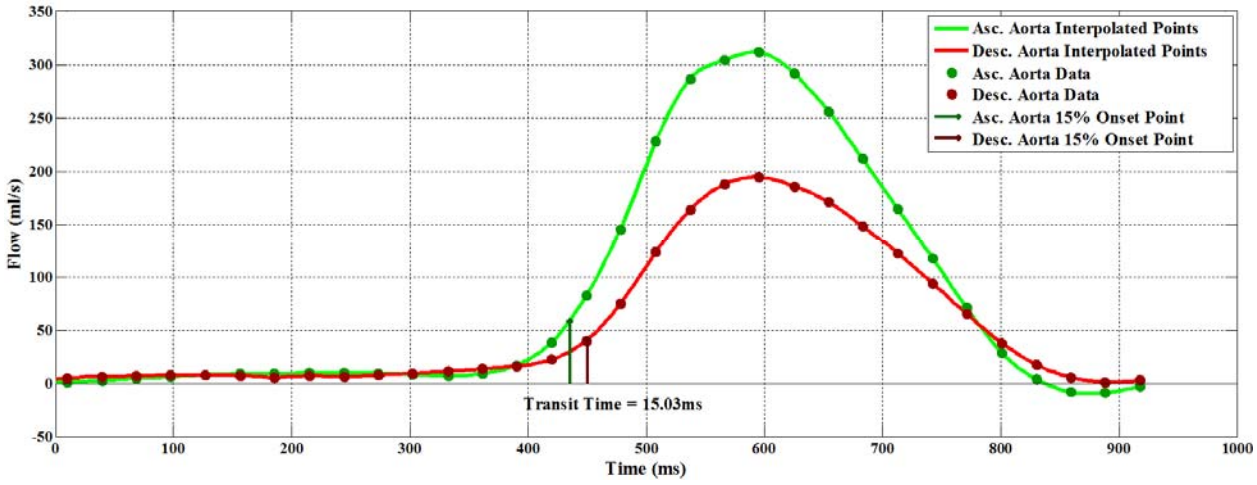


Figure 4.7: Onset time analysis using landmark at 15% of maximum flow

### 4.3.4 Peak Acceleration Analysis

In peak acceleration analysis, the landmark used for comparison is the point at which the rate of flow is at its maximum value. The rate of flow will be at a maximum as the LV is contracting and therefore imparting the largest amount of impulse upon the blood during the cardiac cycle. In order to find this point, the derivative of the flow data must be taken in order to obtain the rate of flow over time. From this new data set, the maximum point is then located for both of the measurement points. The difference in times at which the maximum rates occur is taken as the transit time for PWV calculation. This process is illustrated in Figure 4.8.

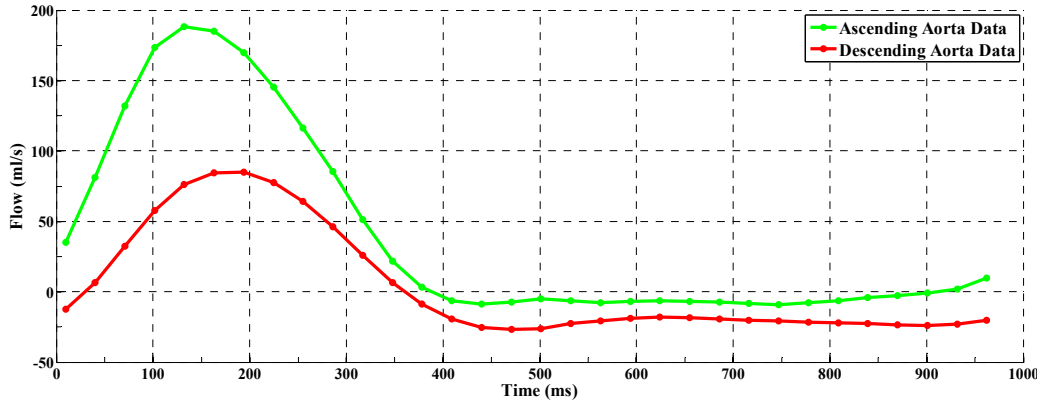


(a)

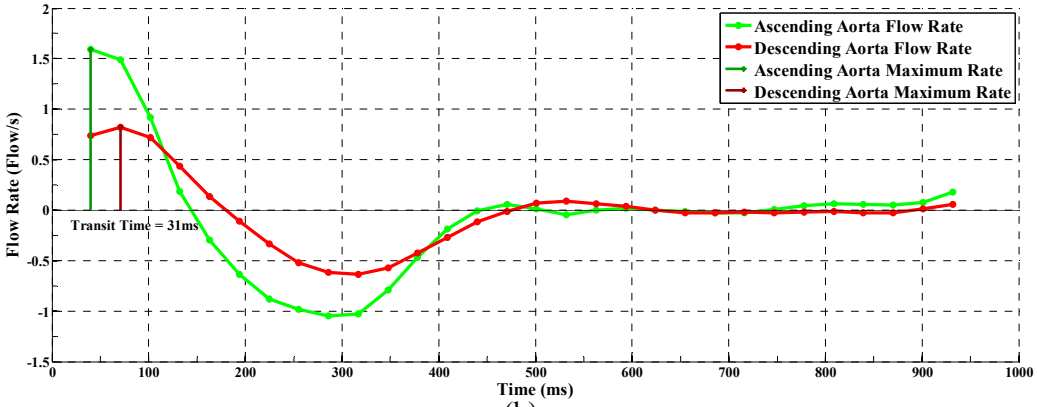


(b)

Figure 4.8: Plots of analysis using the peak acceleration method. Plot (a) is the flow data while plot (b) shows the rate of flow for both measurement points.

### 4.3.5 Issues with Transit Time Determination in the Time Domain

Though these methods are commonly implemented, there are flaws regarding their reliability. These issues stem mainly from the fact that the techniques are adopted from their use with earlier methods such as cardiac catheterization. While the methods are still reasonably viable, the differing nature of MRI and the data it produces causes some problems.

A major issue with PC MRI data is the significantly reduced temporal resolution. This is because the PC MR images require two separate acquisitions with different flow-encoding gradients in order to correct any phase errors. As a result, an image is collected approximately every 30ms. Therefore, in a complete cardiac cycle, approximately 32 data points will be collected. Of these data points, roughly 10 will fall into the pulse wave that exists during systole and be significant in time domain-based analyses.

Any deviation in the quantification of even a single one of the significant points, whether by user error in contouring or due to poor image data, will result in a large error in the calculated transit time and therefore the overall PWV.

On the other hand, catheterization data can have about an order of magnitude higher temporal resolution than that of PC MRI. This can be seen in Figure 4.9. This results in a lessened influence of a single data point on the overall quantification of the flow, allowing for a more precise and accurate quantification. This resolution, combined with its reduced noise and artifacts, is one of the reasons that results from catheterization data are held as gold standard.

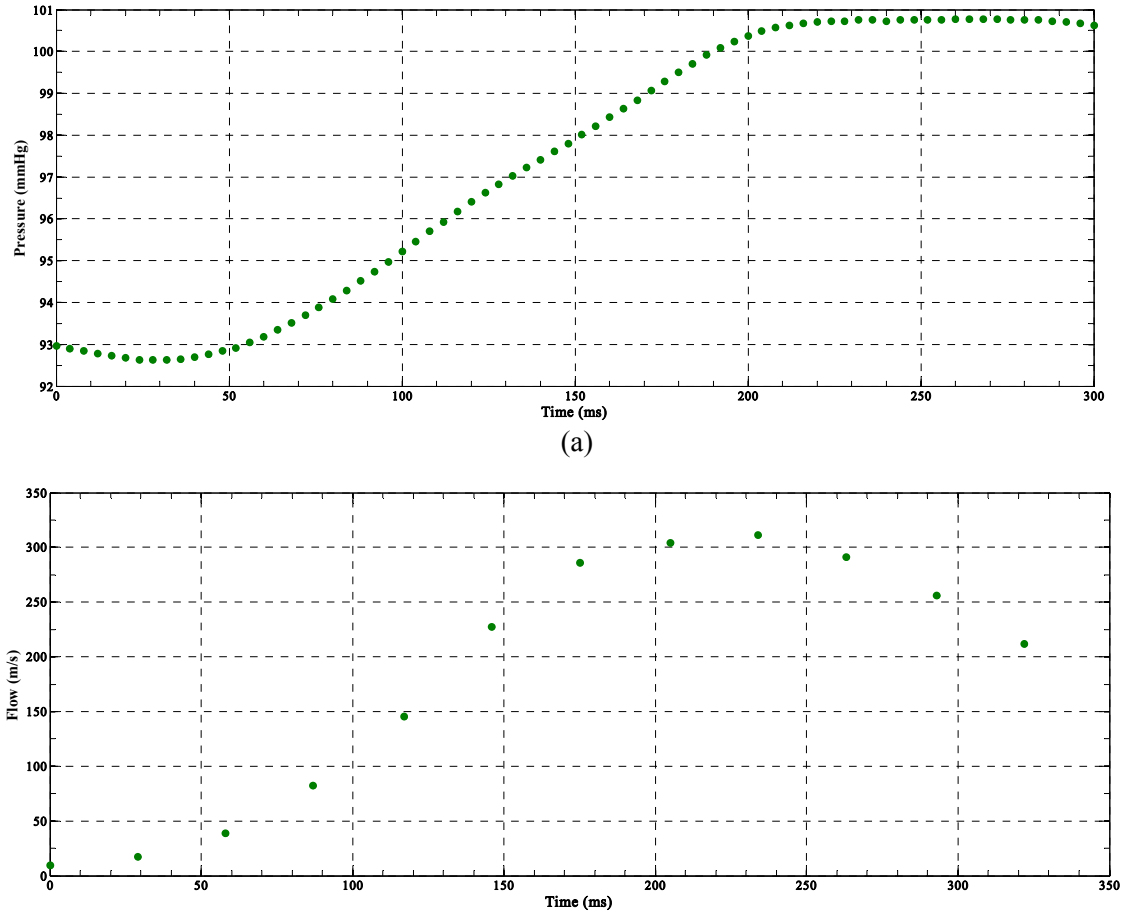


(a)

(b)

Figure 4.9: Comparison of a 300ms portion of data from catheterization (a) and PC MRI (b). The temporal resolution from catheterization data is 4ms while that from PC MRI is 29ms.

The impetus, then, is to find a method that would allow for both more precision and increased accuracy in PWV quantification using PC MRI. This would be done either through increasing the temporal resolution of the scanner output or to find a calculation method that reduces the impact that error in a single data point can cause. An alternative calculation method will be discussed in Section 4.4.

### 4.4 Alternative Method for Transit Time Determination Using the Frequency Domain

It was previously asserted that a major issue with the use of PC MRI data in PWV calculations is the relatively low temporal resolution. A method is proposed where data is first converted from the time domain to the frequency domain before calculating the transit time. This method is similar to one proposed in 1988 by Latson et al. for use with catheterization data [33]. By transferring the data into the frequency domain, all the obtained data points are taken into account, which in turn minimizes the error that can be caused due to a single data point.

This method requires taking the flow profiles of the two points along the artery, $v_{proximal}$ and $v_{distal}$, and using a Fourier transform to convert them into the frequency domain.

$$\mathcal{F}\{v_{proximal}(t)\} = V_{proximal}(\omega) \qquad (4.5)$$

$$\mathcal{F}\{v_{distal}(t)\} = V_{distal}(\omega) \qquad (4.6)$$

From here, a transform function, *H,* can be expressed as the quotient of the two Fourier transforms:

$$H(\omega) = \frac{V_{distal}(\omega)}{V_{proximal}(\omega)} \qquad (4.7)$$

The pulse is assumed to maintain a constant shape as it travels throughout the body. As such, one can assumed a minimized change in the shape of the waveform, allowing the distal point to be expressed as time shifted version of the more promixal point:

$$V_{distal}(\omega) = A \cdot V_{proximal}(\omega) \cdot e^{-2\pi j \Delta t \omega} \qquad (4.8)$$

where *A* is a scale factor. This allows us to substitute this expression for the distal point into Equation 4.7 for the transfer function:

$$H(\omega) = A \cdot e^{-2\pi j \Delta t \omega} \qquad (4.9)$$

Finding the linear phase characteristic of the transfer produces:

$$\angle H(\omega) = -2\pi\Delta t\omega \qquad (4.10)$$

The slope of the linear phase characteristic is $-2\pi\Delta t$, where $\Delta t$ is the transit time between the proximal and distal point. This can then be used to find the value for PWV.

Using this method, the effect of error due to a single point is minimized. Even if there is a change in shape of the waveform between the proximal and distal points of measurement, linear phase characteristic of the transfer function will still remain relatively linear at the lower frequencies as shown in Figure 4.10. This will still allow for accuracy in transit time determination, allowing for a more true determination of PWV.

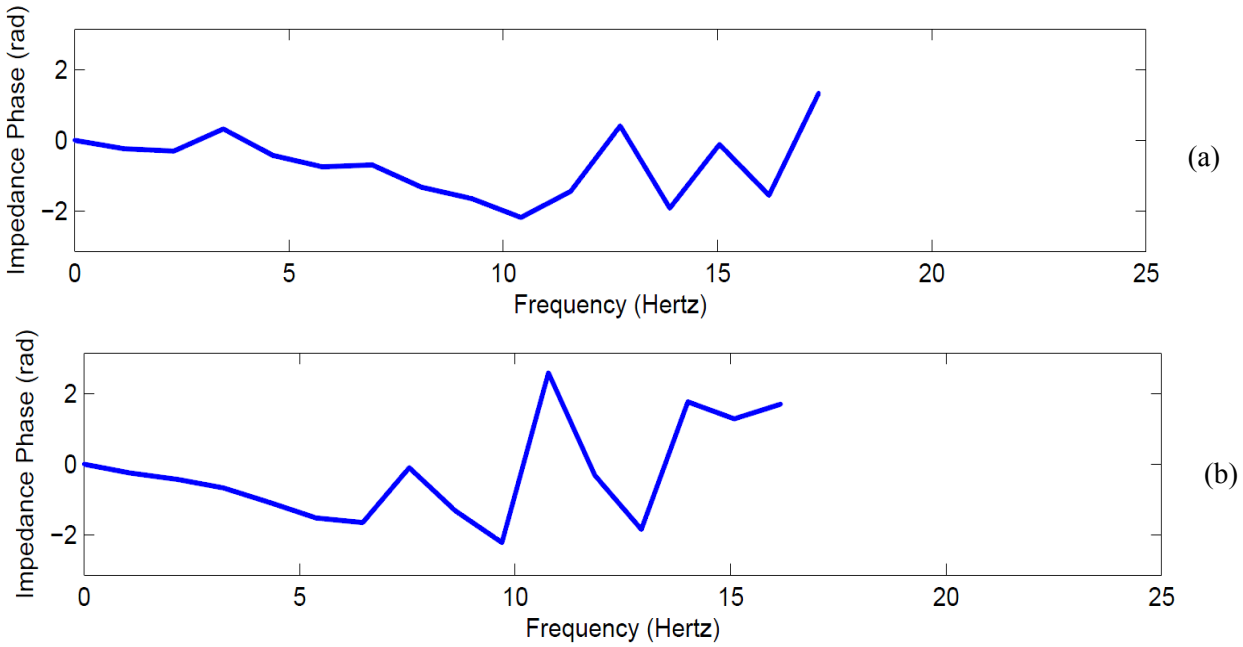


Figure 4.10: Plots of linear phase characteristics used for transit time determination. Plots are included with both a minimal change in waveform shape (a) and a large change in shape (b) between the proximal and distal measurement points.

### 4.5 Comparison of Quantification Methods in Pulse Wave Velocity Calculation

In order to test the validity of the frequency domain approach to transit time determination, PWV calculations were made using the proposed approach and compared to results from point-to-point time domain methods. The subject pool used contained both normal cohorts as well as patients diagnosed with pulmonary hypertension. Subjects with this pathology are known to have an increase in stiffness of the pulmonary arteries. In this validation, there was no gold standard velocity data as catheterization was not performed in relation to this study. Instead, the true velocity is not certain but the differences between the normal and hypertensive hearts was used for validation.

#### 4.5.1 Methodology

The study was conducted (n = 12) using four normal subjects and eight patients with pulmonary hypertension. The subjects underwent cMRI and PC MRI data was acquired from the main pulmonary artery (MPA), proximal to the pulmonary valve, and in the right pulmonary artery (RPA). The studies were conducted with institutional review board (IRB) approval from both Auburn University and the University of Alabama at Birmingham School of Medicine.

The MRI was performed on a 1.5T MRI scanner (CV/i, GE Healthcare, Milwaukee, WI) optimized for cardiac imaging. Free breathing non-segmented cine PC gradient echo was used in order to obtain the necessary flow images of the MPA and RPA cross sections. The parameters of the scan were: a 6mm slice thickness, 32 phases, a 150-200cm/s encoding velocity, field-of-view of 32 x 40cm, scan matrix of 256 x 128, 20° flip angle, NEX of 2-3, 18ms TR, and 5.4ms TE.

After the images were acquired, they were contoured using CAAS MRV software with the method described in Section 4.2. The users manually defined the ROI's as the cross sections of the MPA and RPA. The data was then sent to custom in-house software, where the transit time was determined by both the frequency domain technique as well as point-to-point time domain methods. The specific time domain methods used were onset times at 10%, 20%, 30%, 40%, and 50% onset as well as peak velocity

and peak velocity rate methods. These transit times were then used to calculate PWV in order to get a measure of the arterial stiffness in the pulmonary arteries.

### 4.5.2 Results

The calculated PWVs using transit time determination in the time domain as well as those calculated by the frequency domain method are shown below in Table 4.1.

The results show that there is a large amount of variation between the various time domain based methods for each patient group. The standard error is also considerably larger in the time domain based methods than it is in the frequency domain methods. Also, the difference between the two patient groups did not reach statistical significance when using the time domain methods whereas they were significantly different with the use of the frequency domain methods in calculating transit time.

Table 4.1: PWV (Mean ± Standard Error) measured in m/s from PC-MRI data acquired in the MPA and RPA

| | **Normal** | **Pulmonary Hypertension** | **P vs Normal** |
|---|---|---|---|
| **10%** | -29.6 ± 65.9 | 3.4 ± 1.6 | 0.031 |
| **20%** | 19.3 ± 32.5 | 4.2 ± 1.7 | 0.168 |
| **30%** | 4.3 ± 6.1 | 6.2 ± 2.9 | 0.102 |
| **40%** | 6.4 ± 3.2 | 7.1 ± 3.4 | 0.218 |
| **50%** | 6.3 ± 3.4 | 6.2 ± 3.5 | 0.0928 |
| **Peak** | 6.9 ± 2.9 | 7.8 ± 3.9 | 0.317 |
| **Peak Accel** | 11.6 ± 26.5 | 7.5 ± 4.6 | 0.0883 |
| **Freq** | 4.5 ± 1.3 | 6.3 ± 1.1 | 0.0401 |

### 4.5.3 Discussion

In this section, we attempt to highlight the issues with the time domain methods for PWV calculation and show the efficacy of using a frequency domain based approach.

The large variation between the various time-domain methods is indicative of the problem caused by the low temporal resolution of PC MRI. This is further supported by the large amount of standard error seen in some of the specific time domain based methods such as the 10% and 20% onset time approaches. This also raises the concern of standardization in time-domain based PWV calculations, as the use of a different method results in a largely different result. Finally, the lack of significant difference between the normal subjects and pulmonary hypertensives, a group known to have stiffer arteries, highlights the issue of using such methods for various pathologies.

On the other hand, the frequency-domain method showed a robustness in the face of changes in flow waveform shape as it flows down the artery. This is due to the lessened impact of single data points on the overall calculation of the transit time. Also, the significant difference between the PWV of the pathology from the normal suggests that this approach can be effectively used to quantify the changes that occur in the PWV due to various cardiovascular dysfunctions.

### 4.5.4 Conclusion

The frequency-domain method is a reliable and effective method to calculate PWV. It has been shown to hold various advantages over time-domain methods as a result of its reduced susceptibility to changes as a result of errors from a single data point. The use of the entire waveform also allows for more precise measurements within a subject group as well granting the ability to differentiate the affects of various pathologies on arterial pulse wave velocity.

### 4.6 Further Work

Whilst the frequency domain method has been compared to the time domain based methods, it is also important to validate the method against a gold standard. In these studies, invasive data was not available. In order to evaluate accuracy of noninvasive determination of PWV through PC MRI and the frequency-domain method, invasive data would need to be collected alongside MRI images. The invasive data would provide a gold standard, showing the actual PWV in the artery, and the noninvasive calculation would be checked for accuracy in determining the true value for PWV.

More work should also be done in regards to a variety of approaches in the frequency domain. While the use of the Fourier transform has shown to be effective in regards to reducing issues caused by the low spatial resolution, other transforms and multipliers could be experimented with to see whether error could be further reduced and a more accurate determination achieved.

# Chapter 5

## Quantification of the Left Atrium

Knowledge regarding the left atrium has grown considerably since the advent of noninvasive imaging modalities. The LA has been shown to remodel and change due to various pathologies and cardiovascular events. Therefore, it is important to find an effective method to quantify the atrium. The work in this chapter regarding the quantification method for the LA has been accepted as an abstract in the 21st annual meeting for the International Society of Magnetic Resonance in Medicine [34].

### 5.1 Overview of the Left Atrium

The left atrium (LA), while originally viewed as a passive transport channel between pulmonary veins and the LV, has become increasingly relevant clinically for the prediction and evaluation of cardiovascular disease. This has become all the more so as new technologies and techniques allow for evaluation and quantification of the LA in vivo.

Anatomically, the LA is located superior to the LV, connected by the atrioventricular junction. As explained in Section 2.1.1, it receives blood from the lungs before transferring it to the LV. Unlike the LV, which is more uniform along the short-axis, the LA has a more windsock like shape as can be seen in Figure 5.1. Blood flow between the two chambers is partially regulated by the mitral valve (MV). The LA is defined by smooth muscular walls that vary in thickness based on the specific wall in question. For example the superior wall can be thicker than the lateral and anterior walls by over 1.5mm [35].

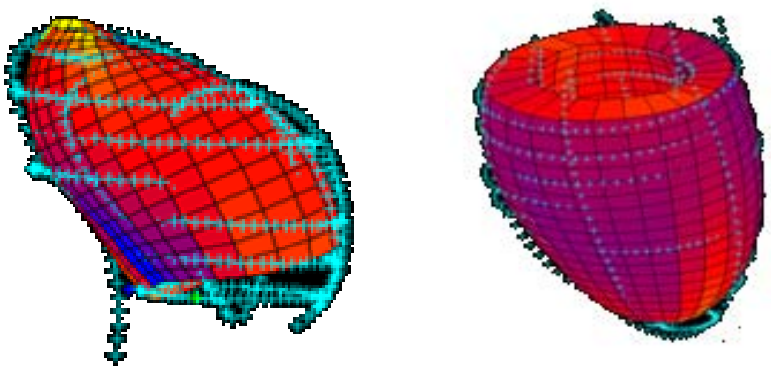

(a) (b)

Figure 5.1: 3D models of LA (a) and LV (b) created using Matlab with contoured 3T cine MRI images.

LA function during the cardiac cycle can be broken down into three main phases, diagrammed in Figure 5.2 below. The first phase, the reservoir phase, corresponds with LV systole and isovolumic relaxation. During this, the LA receives and stores the pulmonary venous return. During the next phase, the LA acts like a conduit and passively transfers blood to the LV. This behavior occurs during early diastole and is theorized to be related to LV suction. In the final phase, corresponding with the final phase of diastole, the LA actively contracts and pumps blood into the LV [36]. This transfer account for approximately 15-30% of the LV stroke volume [37].

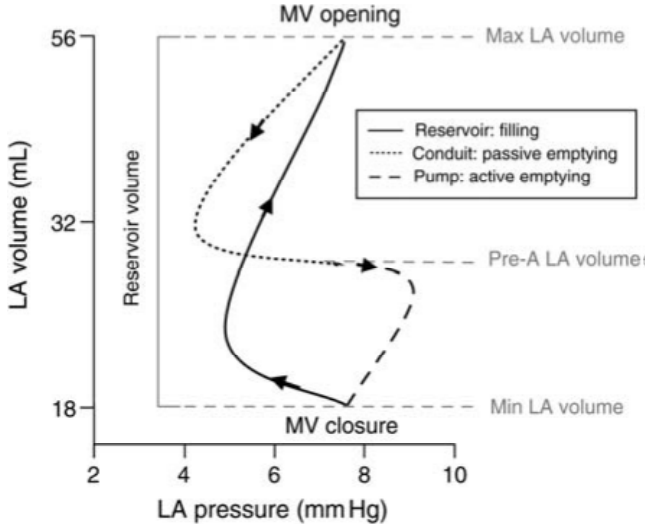


Figure 5.2: LA pressure-volume loop showing the three phases of atrial action during the cardiac cycle [36].

Due to the directly interactive and dynamic relationship between the LA and LV, quantification of the LA allows for clinical evaluation of LV condition. A change in LV stroke volume directly affects both the active and passive emptying volumes of the LA [38]. Also, there is a marked increase in atrial contraction in response to stiffening of the LV. This is further evidenced in studies of heart physiology in response to aging.

As well as allowing clinicians to gain information about the LV, quantification of the LA can help reveal overall cardiovascular health. The majority of atrium related dysfunction originates from the stress and tension of the atrial walls during ejection. However, LA preload, which is volume dependent also plays a role. As there is increased dilation of the LA, the muscle fibers stretch. While these fibers are resilient, some of this stretching becomes permanent. As this is a progressive process, a threshold fiber length can be reached, leading to a decline in shortening and contractility of the LA [39,40]. An indicator of this is atrial volume. Increase in LA volume has been associated with dysfunctions such as stroke [41], congestive heart failure [42], MV disease [43], aortic stenosis [44], and atrial fibrillation [45]. There has also been evidence linking and increase LA volume with aging in terms of general cardiovascular morbidity and mortality [46]. This makes the accurate quantification of LA volume increasingly important both clinically and in research.

### 5.2 Contour Propagation for the Left Atrium

Whilst the imaging protocol for the LA follows a standard cine MRI method, issues do arise when it comes to processing and contouring the images. Drawing contours onto every timeframe is tedious and highly time consuming. As such, methods for propagating contours drawn onto a single timeframe across the entire cardiac cycle were developed. These methods were developed primarily for the ventricles of the heart, primarily the LV. In order to appropriately quantify the LA, its unorthodox geometry, relatively thin walls, mitral annular motion, the presence of pulmonic veins, and the atrial appendage must be taken into account. However these considerations cast doubt onto the efficacy of contour propagation for the LA. Propagation is further made difficult because of the prevalence of flow

artifacts in MRI images of the LA due to its proximity to various blood vessels. In this section, the applicability of a dual contour propagation method is examined.

### 5.2.1 Dual Contour Propagation

In contour propagation, a manually defined contour in a specific timeframe is used to create contours for images along the entire cardiac cycle. In 2009, Wei Feng proposed a geometry independent semi-automated dual-contour propagation that can be applied to both ventricles of the heart [12,47]. This method utilizes contours drawn on both the ES and ED timeframes and propagates them using non-rigid registration (NRR).

In NRR, a template image is used in order to create contours onto a source image through the use of a deformation field. The deformation is computed as the field required to warp the source image to fit onto the template image. The template image will always contain contours either manually drawn or from a previous propagation. The calculated field is then applied to the contours on the template image in order to produce corresponding contours for the source image.

With the dual-contour propagation method, contours drawn on the ES and ED timeframe images are propagated independently via NRR as illustrated in Figure 5.3. The contour from the ED timeframe is propagated forward through systole and backward through diastole up to but not including the ES timeframe. The contours from the ES timeframe are propagated in the same manner, again up to but not including the ED timeframe. These two independent sets of contours are then combined into a single B-spline contour through a weighted least-squares fit. The weight of each set of contours in a specific timeframe is determined by the separation from the manually drawn contour. For a timeframe closer to ES, the weight will be towards the contour propagated from the ES manual contour and less from that propagated from the ED manual contour. This will be reversed for timeframes closer to ED.

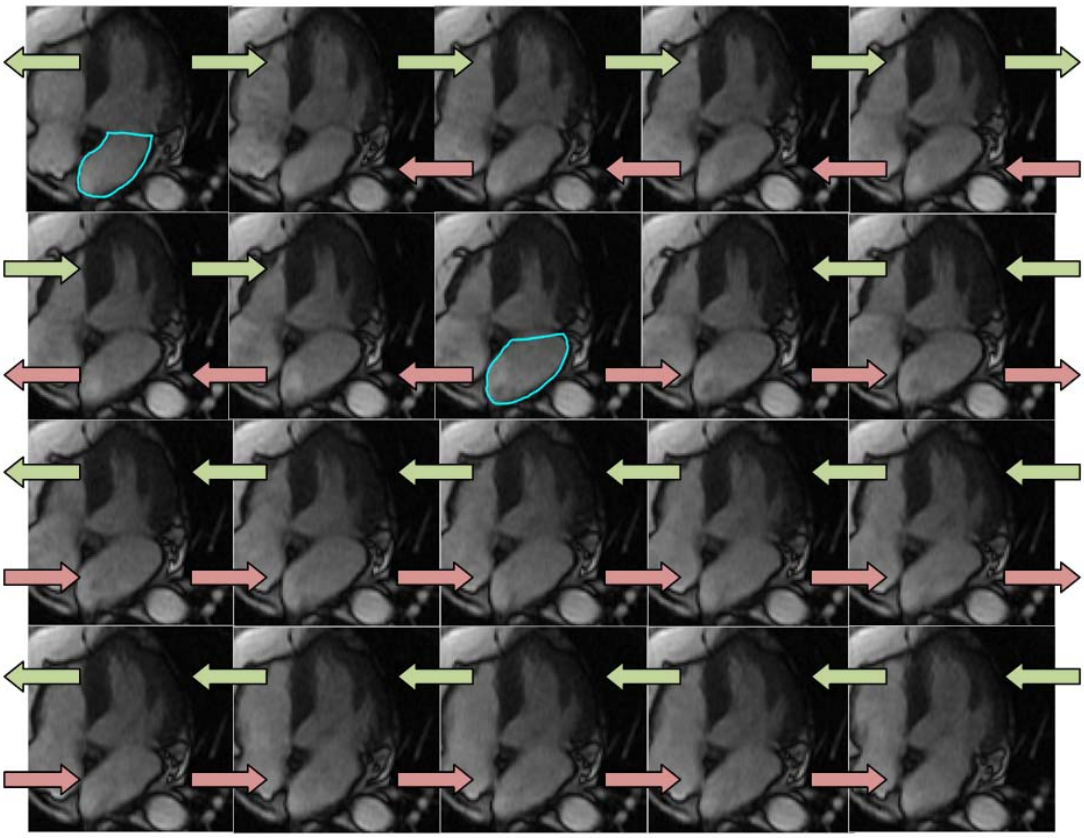

Figure 5.3: Propagation for LA 4ch view as determined by dual-propagation method.

### 5.2.2 Method

To validate the application of the dual-contour propagation method, 10 normal volunteers underwent cMRI. IRB approval was obtained from Auburn University to conduct the study. The subjects were between the ages of 19 and 52, and presented with no cardiac dysfunction. In order to test repeatability, two sets of images were taken, the second between one and four weeks after the initial cardiac scan. Images were taken in the 2ch, 4ch, and SA views taken from the LA apex to a point past the mitral annulus.

The MRIs were performed on a Siemens Verio 3T MRI scanner (Siemens, Erlangen, Germany). A retrospectively-gated breath-hold balanced SSFP sequence was used. The parameters of the scan were: an 8mm slice thickness, field-of-view of 36 x 40cm, a scan matrix 258 x 128, 40° flip angle, 5,4ms TR, and 1.4ms TE.

The images were then contoured using custom in-house software. Contours were drawn on the ED and ES timeframes on all the SA slices as well as on the 2ch and 4ch views. The atrial appendage and pulmonic veins were excluded from the contours based on the adjacent atrial segments. These contours were then propagated using the dual-contour propagation method described in Section 5.2.1. Landmarks were also places on the mitral annulus in order to account for annular motion in calculation.

The contours were then used to calculate LA volume-time curves (VTC) using two separate, already validated methods: the serial short-axis (SSA) method and the area-length (AL) method. These methods are both explained in Section 5.3. The resulting data was then statistically analyzed in order to evaluate validity of the propagated contours. Differences at each timeframe during the cardiac cycle were computed for each method between the two scan times for each of the two methods. Mixed modeling with compound symmetry covariance structure applied to the differences was used for the analysis.

### 5.2.3 Results

The VTCs were computed for both the SSA and AL methods averaged over the study population for each scan. These are shown in Figure 5.4 below.

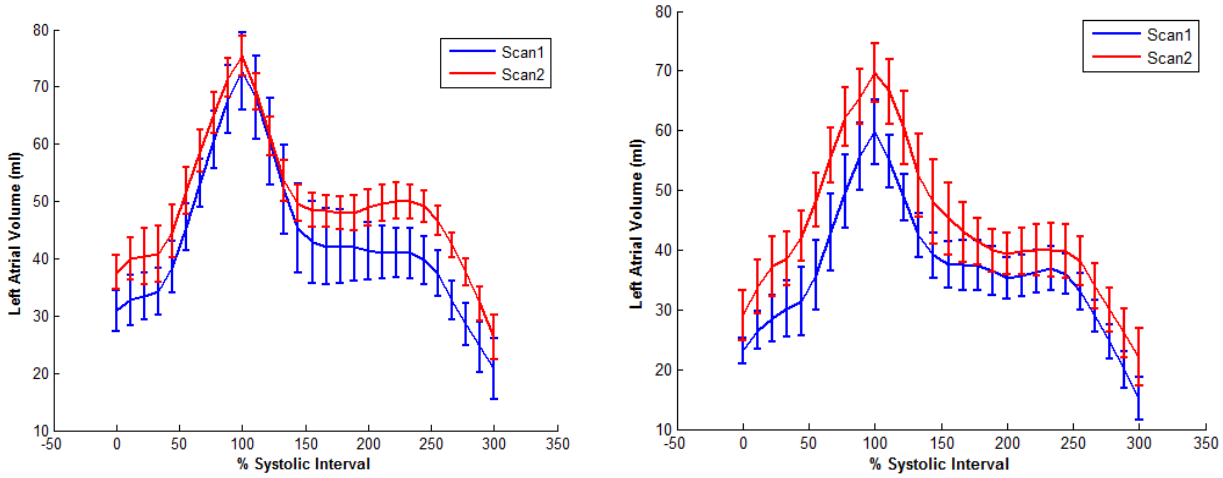


(a) (b)

Figure 5.4: Left atrial volume-time curves averaged over 10 normal subjects computed using the serial short-axis (a) and the area-length (b) methods using two different scans (Scan 1 and Scan 2).

Table 5.1 below shows the least-squares estimate of the mean differences between the two scans for each method. Along with the VTCs, atrial volume, ejection fraction, and rates of filling and ejection were also computed in all the scans using both the SSA and AL methods. There were no significant differences between the two scan times for any of these values. Also, the values were all found to be within an acceptable range for the LA.

Table 5.1: Least-squares estimates of the mean difference in LA volume-time curves between Scan 1 and Scan 2.

| Method | Estimate | Standard Error | DF | t Value | Pr > \|t\| | Alpha | Lower | Upper |
|---|---|---|---|---|---|---|---|---|
| **AL** | 7.3 | 3.8 | 16 | 1.93 | 0.07 | 0.05 | -0.72 | 15.4 |
| **SSA** | 5.7 | 3.8 | 16 | 1.51 | 0.15 | 0.05 | -2.3 | 13. 8 |

### 5.2.4 Discussion

From the results, it can be seen that the dual-contour propagation method can, in fact, accurately be used for the determination of VTCs using both the SSA and AL methods. The results also showed the repeatability when the contouring method was applied for two different scan points. As the methodology called for landmarks placed at the mitral annulus, the VTCs were unaffected by mitral annular motion that would otherwise create difficulties from contours of the LA near the atrioventricular junction. The use of the dual-propagation method is effective in producing LA contours. The fact that manual input is reduced to contouring only the ED and ES timeframes greatly reduces the time spent in post-processing of the cMRI images.

### 5.3 Accepted Methods for Left Atrial Quantification

Due to its ubiquity, the current gold standard for LA quantification is through the use of an echocardiogram [48]. However, cMRI, providing an increased resolution and temporal clarity, has the potential to provide much more accurate results. The two most commonly used LA quantification methods with cMRI data are adopted from methods accepted by the American Society of Echocardiography as being accurate [49]. These methods are the area-length method and the serial short-axis method.

#### 5.3.1 Serial Short-Axis Method

The SSA method is considered the relatively more accurate method of quantifying the LA. In this method, MRI images of the atrium are taken along the short-axis. These images are then contoured and the summation of these contours is taken as the volume for the LA. It is due to this comprehensive nature that the SSA method is considered the most reliable.

While it is indeed more comprehensive, this leads to an increased amount of time needed for imaging and post-processing. Obtaining SA images is time intensive due to the number of images taken. It also requires more breath-holds from subjects in the MRI which can be problematic when dealing with cardiovascular pathologies. There is also an increased amount of time required in post-processing due to the sheer number of images that need to be contoured in order to obtain volume data.

#### 5.3.2 Area-Length Method

The AL method was developed as a less time and process intensive method for LA quantification. Unlike the SSA, this method only requires a 2ch and a 4ch image. Contouring both sets of images provides an area for each view. The model then assumes a prolate ellipsoid geometry for the LA and calculates volume as:

$$V_{LA} = \frac{8}{3\pi} \cdot \frac{A_{2ch} \cdot A_{4ch}}{L} \qquad (5.1)$$

where $A_{2ch}$ and $A_{4ch}$ are the corresponding areas for each of the views, and $L$ is the length of the LA defined as the distance from the mitral annulus to the posterior LA wall [49]. As a value for $L$ will given from each of the 2ch and 4ch views, the shortest of these values is taken to be the atrial length. This process is illustrated below in Figure 5.5.

This method, whilst being much less time consuming than the SSA does make some sacrifices in regards to accuracy. The primary issue arises with determination for atrial length as there can be inconsistencies. There is also the use of a prolate ellipsoid that may cause inaccuracies with the volume determination. The LA is a more unorthodox shape and the use of such a geometry can result in overestimation of volume. Lastly, it has been shown that the atrium assumes a more cylindrical shape as it enlarges [50] and so the AL method may be unreliable in LA quantification for various pathologies.

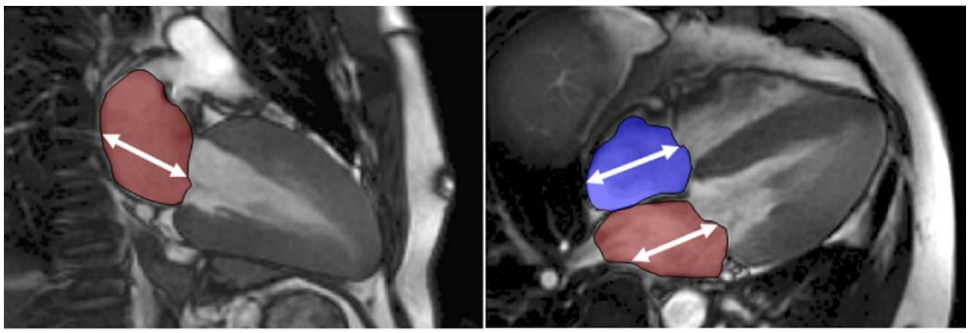

(a) (b)

Figure 5.5: 2ch (a) and 4ch (b) used to calculate area and length. The LA area is represented in red with the white arrow showing the length of the atrium [51].

### 5.4 Proposed Virtual Short-Axis Method for Left Atrial Quantification

In this section, a virtual short-axis (VSA) method is proposed to find LA volume. This new method is an attempt to balance the benefits of both the AL and SSA methods whilst minimizing the issues that they both have. The VSA method uses only the 2ch and 4ch images, thus avoiding the time consumption caused by acquiring and processing short-axis data. It also seeks to eliminate the error that can arise from geometric assumptions like those of the AL method.

In this method, the contours from the 2ch and 4ch views are used as boundaries to create a series of virtual short-axis elliptical discs. These discs are set at 0.5mm distances from each other. As the 2ch and 4ch views are roughly orthogonal, corresponding diameters of the contours at the .5mm intervals are set as the major and minor axes of the ellipse. The diameters are computed by use of a line from the mitral annulus to the LA posterior wall which acts as the center. The diameters are calculated to be the width across the contour at each interval perpendicular to that center. The areas are then summed to determine the LA volume.

### 5.5 Validation of the Virtual Short-Axis Method

The VSA method while promising, does need to be validated. In order to do so, LA VTCs are computed using each of the three aforementioned methods. Using the results of the SSA method as the most accurate VTC's from the data from the AL and VSA methods are compared with relation to the SSA results.

#### 5.5.1 Method

The validation was conducted using nine healthy volunteers between the ages of 19 and 52. These subjects presented with no known cardiac dysfunction at the time of cMRI. Auburn University IRB approval was obtained for this study. Slices were taken in the 2ch, 4ch, and 6-8 slices along the short-axis from the LA apex to a point approximately 1.5cm distal to the mitral annulus.

The MRIs were performed on a Siemens Verio 3T MRI scanner (Siemens, Erlangen, Germany). A retrospectively-gated breath-hold balanced SSFP sequence was used. The parameters of the scan were: an 8mm slice thickness, field-of-view of 36 x 40cm, a scan matrix 258 x 128, 40° flip angle, 5,4ms TR, and 1.4ms TE.

Contours were manually drawn using custom in-house software at the ED and ES timeframes on the 2ch, 4ch. and each of the slices in the short-axis views. These contours were then propagated to the

other timeframes using the method defined in Section 5.2.1. From here, LA VTCs were computed using each of the three methods: the AL, SSA, and VSA method.

For the analysis, results from the SSA method were considered to be the gold standard. In order to validate the VSA method, the hypothesis tested was that VTCs from the VSA method are closer to the SSA VTCs than those computed by the AL method. This was done by computing the differences between the two methods against the SSA: AL-SSA and VSA-SSA. Compound symmetry covariance structure was applied to the differences and these were compared using mixed modeling. Finally, the absolute differences were also compared using mixed modeling with applied compound symmetry covariance.

### 5.5.2 Results

Figure 5.6 shows the VTCs of each of the three methods averaged over the nine subjects. The shapes of the VTCs are all qualitatively similar. The results from the comparison of the mean differences of the AL and VSA methods from the SSA data are shown in Table 5.2. In Table 5.3, the least-squares estimates of the difference between the absolute differences |VSA-SSA| and |AL - SSA| are displayed.

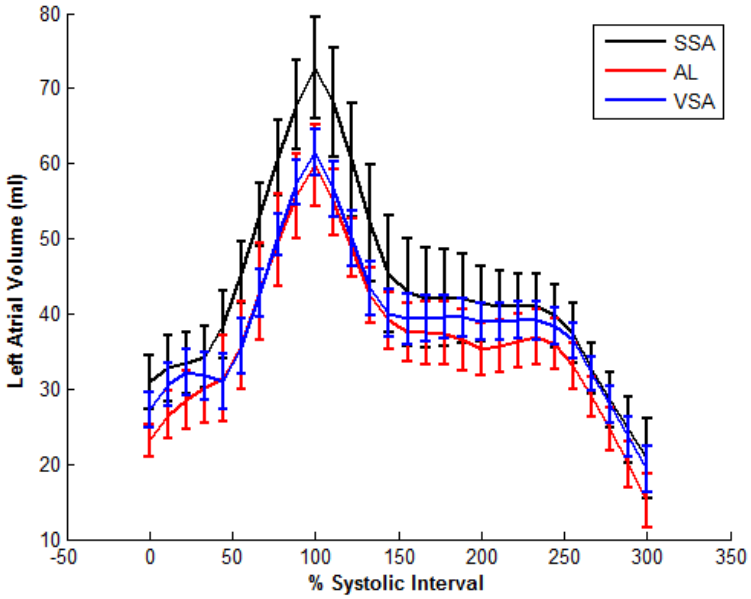


Figure 5.6: VTCs averaged over nine normal human volunteers computed using serial short-axis (SSA), area-length method (AL) and virtual short axis (VSA).

Table 5.2: Least-squares estimates of the mean differences between VTCs computed in ml using VSA and AL compared to SSA

| | Estimate | Standard Error | DF | t Value | Pr > \|t\| | Alpha | Lower | Upper |
|---|---|---|---|---|---|---|---|---|
| **AL-SSA** | -5.7 | 3. 8 | 24 | -1.52 | 0.14 | 0.05 | -13. 5 | 2.1 |
| **VSA-SSA** | -6.2 | 3. 8 | 24 | -1.66 | 0.11 | 0.05 | -14 | 1.5 |

Table 5.3: Least square estimate of the mean difference in ml between |AL-SSA| and |VSA-SSA| VTCs

| | **\|AL-SSA\|-\|VSA-SSA\|** |
|---|---|
| **Estimate** | 6.8 |
| **Std Error** | 0.83 |
| **DF** | 8 |
| **t Value** | 8.12 |
| **Pr > \|t\|** | <.0001 |
| **Adjustment** | Tukey-Kramer |
| **Adj P** | <.0001 |
| **Alpha** | 0.05 |
| **Lower** | 4.8 |
| **Upper** | 8.7 |
| **Adj Lower** | 4.8 |
| **Adj Upper** | 8.7 |

### 5.5.3 Discussion

From the least-squares estimates of the differences shown in Table 5.2, it is revealed that there is no significant difference in either of these methods from the SSA method results. As the AL method has been accepted as a valid method for LA quantification, it extends that as the VSA method produces VTCs that are as significantly close to those from the SSA method as the results from the AL method, VSA is also a valid method.

Meanwhile Table 5.3 illustrates that the absolute difference between the AL and SSA methods is significantly higher than that found between the VSA and SSA methods. This shows that the VSA method is potentially a more reliable method than using AL. This is also quantitatively evidenced by

Figure 5.6 where the mean VTC from the VSA method is closer to that of the SSA than the mean VTC from the AL method.

It is important to note that while the SSA method was used as the standard for comparison, it has not been validated against anatomical standard to claim it as a gold standard. There are concerns to be raised as a 6-10mm slice thickness and the difficultly in defining the boundary between the pulmonary veins and the LA in the short axis views. Therefore, there is a chance of misestimating the true atrial volume. However, due to its comprehensive nature, it is considered a 3D technique and the most accurate determination of LA volume using cMRI.

Therefore from this data, it can be said that the VSA method is effective in quantifying LA volumes. It is more effective in its use of the 2ch and 4ch views than the AL method while still avoiding the extra processing time required by the SSA method.

### 5.6 Conclusion and Further Work

In this section, a more effective method quantification method for the left atrium was sought. This attempt came in two parts: the improvement of post-processing technique and a more effect method for volume quantification.

The attempt to improve post-processing technique came in the application of a dual-contour propagation method to more efficiently contour the LA. As contouring over all timeframes it very tedious and time-intensive, the method would need only the ED and ES timeframes contoured manually, saving a lot of time. While this method has been previously validated in the LV and RV, its effectiveness in the LA had not been determined. However, through evaluation it has been found to indeed be an effective propagation tool. This allowed for a quicker and more thorough testing of quantification methods.

The VSA method was introduced as a more effective alternative to the AL method for LA volume quantification. While the AL technique eliminated the time-consuming use of short-axis contours, there have been doubts as to the accuracy of its geometric assumptions. Through the use of the VSA method,

these geometric assumptions were eliminated and it was shown to be an effective method in LA quantification.

It is important to note that these studies were all done using normal volunteers. While there was some diversity in subject age, this was neither carefully controlled nor taken into account. As such, the efficacy of both the propagation technique and the VSA method will need to be evaluated in regards to subject age and with various pathologies. As the atrium is wont to remodel in both cases, the applicability of these technique will need to be evaluated through further research. For further validation, comparison of volumes calculated from this method with LA volumes for the same subject obtained using cardiac CT would be beneficial.

# Chapter 6

## Summary and Future Work

The cardiovascular system plays an essential role in the human body. In order to get a comprehensive perspective on the overall system, the individual components must first be characterized. In this thesis, the quantification of two particular aspects of the cardiovascular system using cMRI was discussed: blood flow in the arteries and left atrial volume.

With regards to blood flow in the arteries, prevalent time-domain based methods to quantify flow through the use of PWV were discussed. The shortcomings in the use of these methods with PC MRI data were presented and an alternative, frequency-domain based method for PWV determination was examined. This method was shown to be more robust and reliable as it compensated for the relatively low temporal resolution of PC MRI data.

In this thesis, LA quantification was approached in two ways: post-processing technique and volumetric quantification methodology. In regards to post-processing, the applicability to a dual-contour propagation method on the LA was evaluated. This technique, previously validated for the LV and RV, was shown to be a viable method of contouring LA images. By reducing the manual tasks to solely needing to contour the ED and ES timeframes, a lot of time can be saved in preparing the images for quantification. Volumetric analysis of the LA was also explored. The AL and SSA methods, both adopted for MRI use from echocardiography techniques, were discussed. The issues with the use of these techniques were discussed and a novel VSA method was proposed. This method allowed for more accurate quantification through the dismissal of inaccurate geometric assumptions while still minimizing the number of cMRI images that need to be collected and processed. The VSA method was shown be a valid method that can be more accurate in quantification than the AL method. It also holds promise in regards to accurate quantification of remodeled atria.

It should be noted that the majority of this work was done using subjects who did not present with cardiovascular dysfunction. However such issues, along with aging, change the physical and

physiological characteristics of cardiovascular anatomy. Therefore, the further applicability of all the methods presented should be explored with regards to modified cardiac anatomy.

The work in this thesis is a portion of the groundwork for a more comprehensive characterization of the cardiovascular system. Cardiovascular diseases and events are usually looked at in the specific vessels and chambers. By analyzing the rest of cardiovascular system in addition to the specifically affected one, a more complete perspective of cardiovascular interactions can be gleaned. In order to do this, effective quantification methods for the other chambers and vessels should be pursued. While there has been a lot of work on the ventricles, the contribution of the more peripheral structures such as the atrial appendage can be quantified. When more complete quantification is done, the characteristics of different structures can be compared and the interactions between the different anatomies can be more specifically defined.

## References


[1] Marieb E.N, Hoehn K, *Human Anatomy and Physiology 8th ed.*, 2010. Pearson Education Inc.

[2] "*http://www.lpch.org*"

[3] Klabunde RE, *Cardiovascular Physiology Concepts 2nd ed.,* 2012 Lippincott Williams and Wilkins

[4] "*http://fau.pearlashes.com*"

[5] "*http://www.antranik.org*"

[6] "*http://www.urgomedical.cn*"

[7] National Institute of Medicine, *Promoting Cardiovascular Health in the Developing World : A Critical Challenge to Achieve Global Health*. 2010 Washington, D.C.: National Academies Press

[8] McMurray JJV, Pfeffer MA, *Heart Failure.* The Lancet, 2005. 365(9474): p. 1877-1889

[9] "*http://fmrib.ox.ac.uk*"

[10] Li J, *Tag line tracking and cardiac motion modeling from tagged MRI,* Ph.D. dissertation, Auburn University, 2006.

[11] Lee V.S, *Cardiovascular MRI: physical principles to practical protocols.* 2006. Lippincott Williams & Wilkins

[12] Zha, Wei. *Novel Techniques for Measuring Cardiac Shape and Mechanics with Magnetic Resonance Imaging*. Ph.D dissertation, Auburn University, 2012

[13] Jha N, Zha W, Gupta H, Lloyd S, Denney TS. *Quantification of Pulse Wave Velocity From Phase-Contrast MRI Data Using Fourier Analysis [abstract]*. ISMRM 20th Annual Meeting & Exhibition. ISMRM; 2011. Abstract nr 3913.

[14] Nichols WW, O'Rourke MF, *McDonald's Blood Flow in Arteries, Theoretical, experimental and clinical principles*. Arnold, London, fourth edition. 1998.

[15] Belz GG, *Elastic properties and windkessel function of the human aorta*. Cardiovascular Drugs Ther. 1995;9(1):73–83.

[16] Chao-Wang Chen; Shau, Y.-W.R.; Chien-Ping Wu, *Analog transmission line model for simulation of systemic circulation* Biomedical Engineering, IEEE Transactions on , vol.44, no.1, pp.90,94, Jan. 1997

[17] Dogui et al. *Consistency of aortic distensibility and pulse wave velocity estimates with respect to the Bramwell-Hill theoretical model: a cardiovascular magnetic resonance study*. Journal of Cardiovascular Magnetic Resonance 2011 13 :11.

[18] Redheuil A et al. *Reduced ascending aortic strain and distensibility: earliest manifestations of vascular aging in humans.* Hypertension. *2010;55:319–326.*

[19] Mitchell GF, Pfeffer MA, *Pulsatile hemodynamics in hypertension*. Curr Opin Cardiol. 1999;

[20] Cruickshank K, Riste L, Anderson SG, Wright JS, Dunn G, Gosling RG, *Aortic pulse wave velocity and its relationship to mortality in diabetes and glucose intolerance: an integrated index of vascular function* Circulation. 2002

[21] Blacher J, Asmar R, Djane S, London G, Safar M, *Aortic pulse wave velocity as a marker of cardiovascular risk in hypertensive patients.* Hypertension. 1999a;33(5):1111.

[22] Laurent S, Boutouyrie P, Asmar R, Gautier I, Laloux B, Guize L, Ducimetiere P, Benetos A, *Aortic stiffness is an independent predictor of all-cause and cardiovascular mortality in hypertensive patients*. Hypertension. 2001a;37(5):1236–41.

[23] Blacher J, Guerin A, Pannier B, Marchais S, Safar M, London G, *Impact of aortic stiffness on survival in end-stage renal disease.* Circulation. 1999b;99(18):2434.

[24] Mattace-Raso FU, van der Cammen TJ, van der Meer IM, Schalekamp MA, Asmar R, Hofman A, Witteman JC, *C-reactive protein and arterial stiffness in older adults: the Rotterdam Study.* Atherosclerosis. 2004;176(1):111–6.

[25] Herrington DM, Brown WV, Mosca L, Davis W, Eggleston B, Hundley WG, Raines J, *Relationship between arterial stiffness and subclinical aortic atherosclerosis*. Circulation. 2004;110(4):432–437.

[26] Boutouyrie P, Tropeano AI, Asmar R, Gautier I, Benetos A, Lacolley P, Laurent S*, Aortic stiffness is an independent predictor of primary coronary events in hypertensive patients: a longitudinal study.* Hypertension. 2002;39(1):10–15.

[27] Laurent S, Boutouyrie P*, Recent advances in arterial stiffness and wave reflection in human hypertension*. Hypertension. 2007;49(6):1202–1206.

[28] Laurent S, Katsahian S, Fassot C, Tropeano AI, Gautier I, Laloux B, Boutouyrie P, *Aortic stiffness is an independent predictor of fatal stroke in essential hypertension*. Stroke. 2003;

[29] Meaume S, Benetos A, Henry OF, Rudnichi A, Safar ME, *Aortic pulse wave velocity predicts cardiovascular mortality in subjects >70 years of age*. Arterioscler Thromb Vasc Biol. 2001;21(12):2046–50.

[30] Mancia G et al. *Guidelines for the management of arterial hypertension: The task force for the management of arterial hypertension of the European Society of Hypertension (ESH) and of the European Society of Cardiology (ESC)*. J Hypertens. 2007

[31] "*http://www.math.ucla.edu*"

[32] Srichai, M. B., Lim, R. P., Wong, S., & Lee, V. S. *Cardiovascular Applications of Phase-Contrast MRI.* American Journal of Roentgenology, 192(3), 662–675. 2009.

[33] Latson, TW et al . *Effect of nitroglycerin on aortic impedance, diameter, and pulse-wave velocity.* Circulation Research 1988, 62:884-890

[34] Jha N, Schiros C, Salibi N, Gupta H, Lloyd S, Dell'Italia LJ, Denney TS. *Virtual Short Axis: A Novel Method for Computing Left Atrial Volumes from Two and Four Chamber MRI [abstract]*. ISMRM 21st Annual Meeting & Exhibition. ISMRM; 2012. Abstract nr 4503.

[35] Ho SY, Cabrera JA, Sanchez-Quintana D. *Left Atrial Anatomy Revisited*. Circ Arrhythm Electrophysiol. 2012;5:220-228.

[36] Blume GG, et al. *Left Atrial Function: Physiology, Assessment, and Clinical Implications.* European Journal of Echocardiography 2011;12:421–430

[37] Pagel PS, Kehl F, Gare M, Hettrick DA, Kersten JR, Warltier DC. *Mechanical function of the left atrium: new insights based on analysis of pressure–volume relations and Doppler echocardiography.* Anesthesiology 2003;98:975–94.

[38] Erol MK, Ugur M, Yilmaz M, Acikel M, Sevimli S, Alp N. *Left atrial mechanical functions in elite male athletes*. Am J Cardiol 2001;88:915–7, A9.

[39] Sunagawa K, Maughan WL, Burkhoff D, Sagawa K. *Left ventricular interaction with arterial load studied in isolated canine ventricle.* Am J Physiol 1983;245(Pt 1):H773–80.

[40] Stone HL. *Effect of heart rate on left atrial systolic shortening in the dog*. J Appl Physiol 1975;38:1110–6.

[41] Tsang TS, Barnes ME, Gersh BJ, Bailey KR, Seward JB, *Left atrial volume as a morphophysiologic expression of left ventricular diastolic dysfunction and relation to cardiovascular risk burden* Am J Cardiol, 90 (2002), pp. 1284–1289

[42] Kizer JR, Bella JN, Palmieri V, Liu JE, Best LG, Lee ET, Roman MJ, Devereux RB, *Left atrial diameter as an independent predictor of first clinical cardiovascular events in middle-aged and elderly adults: the Strong Heart Study (SHS)* Am Heart J, 151 (2006), pp. 412–418

[43] Chandran CB, Kitchin AH, *Left atrial volume changes in mitral valve disease: A cross-sectional echocardiographic study* Eur. Heart J., 8 (1987), pp. 888–894

[44] Stott DK, Marpole DGF, Bristow JD, Kloster FE, Griswold HE, T*he role of left atrial transport in aortic and mitral stenosis* Circulation, 41 (1970), pp. 1031–1041

[45] Sanfilippo AJ, Abascal VM, Sheehan M et al *Atrial enlargement as a consequence of atrial fibrillation. A prospective echocardiographic study* Circulation, 82 (1990), pp. 792–797

[46] Thomas L, Levett K, Boyd A, Leung DY, Schiller NB, Ross DL. *Changes in regional left atrial function with aging: evaluation by Doppler tissue imaging*. Eur J Echocardiogr 2003;4:92–100.

[47] Feng, W., *Global and Local Cardiac Functional Analysis with Cine MR Imaging: A Non-Rigid Image Registration Approach.* Ph.D dissertation, Auburn University, 2009.

[48] Hudsmith LE, Petersen SE, Francis JM, Robson MD, Neubauer *S. Normal human left and right ventricular and left atrial dimensions using steady state free precession magnetic resonance imaging*. J Cardiovasc Magn Reson 2005; 7:775-782

[49] Lang RM, Bierig M, Devereux RB, et al. *Recommendations for chamber quantification: a report from the American Society of Echocardiography's Guidelines and Standards Committee and the Chamber Quantification Writing Group, developed in conjunction with the European Association of Echocardiography, a branch of the European Society of Cardiology*. J Am Soc Echocardiogr 2005; 18:1440-1463.

[50] Rodevan O, et al. *Left atrial volumes assessed by three- and two-dimensional exhoxardiography compared to MRI estimates.* International J Card Imaging 1999 15(5): 397-410

[51] Whitlock, Matthew, et al. *Comparison of left and right atrial volume by echocardiography versus cardiac magnetic resonance imaging using the area-length method.* The American journal of Cardiology 106.9 (2010): 1345-1350